



1 **The 2019 Raikoke eruption as a testbed for rapid assessment of**  
2 **volcanic atmospheric impacts by the Volcano Response group**

3

4 Jean-Paul Vernier<sup>1,2</sup>, Thomas J. Aubry<sup>4</sup>, Claudia Timmreck<sup>3</sup>, Anja Schmidt<sup>5,5b,5c</sup>, Lieven  
5 Clarisse<sup>6</sup>, Fred Prata<sup>7</sup>, Nicolas Theys<sup>8</sup>, Andy T. Prata<sup>9,\*</sup>, Graham Mann<sup>10</sup>, Hyundeok Choi<sup>11</sup>,  
6 Simon Carn<sup>12</sup>, Richard Rigby<sup>13</sup>, Susan C. Loughlin<sup>14</sup> and John A. Stevenson<sup>14</sup>

7

8 (1) National Institute of Aerospace, Hampton, VA 23692

9 (2) NASA Langley Research Center, Hampton, VA 23692

10 (3) Max-Planck-Institut für Meteorologie, Hamburg, Germany

11 (4) Department of Earth and Environmental Sciences, University of Exeter, Penryn, UK

12 (5) Institute of Atmospheric Physics (IPA), German Aerospace Center (DLR), Oberpfaffenhofen, German

13 (5b) Meteorological Institute, Ludwig Maximilian University of Munich, Munich, Germany

14 (5c) Department of Chemistry, University of Cambridge, Cambridge, United Kingdom

15 (6) Université libre de Bruxelles (ULB), Service de Chimie Quantique et Photophysique, Atmospheric  
16 Spectroscopy, Brussels, Belgium

17 (7) AIRES Pty Ltd, Mt Eliza, Victoria, Australia

18 (8) Royal Belgian Institute for Space Aeronomy (BIRA-IASB), Brussels, Belgium

19 (9) Sub-Department of Atmospheric, Oceanic and Planetary Physics, University of Oxford, Oxford OX1 3PU, UK.

20 \*now at School of Earth, Atmosphere and Environment, Monash University, Clayton, Victoria 3800, Australia.

21 (10) University of Leeds, Leeds, UK.

22 (11) Science Applications International Corporation, Inc. (SAIC) at NOAA/NWS/NCEP/Environmental Modeling  
23 Cent

24 (12) Michigan Tech, USA

25 (13) Centre for Environmental Modelling and Computation, School of Earth and Environment, University of Leeds,  
26 UK

27 (14) British Geological Survey, Edinburgh, UK

28

29 *Correspondence to: Jean-Paul Vernier (jeanpaul.vernier@gmail.com)*

30

31

32



33 **Abstract.** The 21<sup>st</sup> June 2019 Raikoke eruption (48°N,153°E) generated one of the largest amounts of sulfur emission  
34 to the stratosphere since the 1991 Mt Pinatubo eruption. Satellite measurements indicate a consensus best estimate of  
35 1.5 Tg for the sulfur dioxide (SO<sub>2</sub>) injected at an altitude of around 14-15 km. The peak northern hemisphere mean  
36 525nm Stratospheric Aerosol Optical Depth (SAOD) increased to 0.025, a factor of three higher than background  
37 levels. The Volcano Response (VolRes) initiative provided a platform for the community to share information about  
38 this eruption, which significantly enhanced coordination efforts in the days after the eruption. A multi-platform  
39 satellite observation sub-group formed to prepare an initial report to present eruption parameters including SO<sub>2</sub>  
40 emissions and their vertical distribution for the modelling community. It allowed to make the first estimate of what  
41 would be the peak in SAOD one week after the eruption using a simple volcanic aerosol model. In this retrospective  
42 analysis, we show that revised volcanic SO<sub>2</sub> injection profiles yield a higher peak injection of the SO<sub>2</sub> mass. This  
43 highlights difficulties in accurately representing the vertical distribution for moderate SO<sub>2</sub> explosive eruptions in the  
44 lowermost stratosphere due to limited vertical sensitivity of current satellite sensors (+/- 2 km accuracy) and low  
45 horizontal resolution of lidar observations. We also show that the SO<sub>2</sub> lifetime initially assumed in the simple aerosol  
46 model was overestimated by 66%, pointing to challenges for simple models to capture how the life cycle of volcanic  
47 gases and aerosols depends on the SO<sub>2</sub> injection magnitude, latitude and height. Using revised injection profile,  
48 modelling results indicate a peak northern hemisphere monthly mean SAOD at 525nm of 0.024, in excellent agreement  
49 with observations, associated with a global monthly mean radiative forcing of -0.17 W/m<sup>2</sup> resulting in an annual global  
50 mean surface temperature anomalies of -0.028 K. Given the relatively small magnitude of the forcing, it is unlikely  
51 that the surface response can be dissociated from surface temperature variability.

## 52 **1. Introduction.**

53 After 95 years of dormancy, the Raikoke volcano in the Kuril Islands (North-West Pacific; 48.292°N, 153.25°E)  
54 began a series of explosions at 18UTC on 21 June 2019 lasting around 24 hours. Raikoke forms a small uninhabited  
55 Island of 2 km x 2.5 km which belongs to the Russian federation, 16 km from Matua Island in the Sea of Okhotsk.  
56 Its name originates from the ancient Japanese Ainu language and translate to “hellmouth” referring to past volcanic  
57 eruptions. The first eruption reports of Raikoke originated from the mid-18<sup>th</sup> century but it was during the 1788  
58 eruption that one third of the Island was destroyed (Gorshkov, 1970). The last known eruption was reported in  
59 February 1924. Since then, the volcano remained dormant. The volcano is monitored by the Sakhalin Volcanic  
60 Eruption Response Team (SVERT) part of the Institute of marine geology and the Kamchatka Volcanic Eruption  
61 Response Team (KVERT). During the latest 2019 eruption, the first explosion of a series of 8 was reported by  
62 KVERT on 21 June at 17h50 UTC and quickly followed 1h later by a volcanic ash advisory produced by the Tokyo  
63 Volcanic Ash Advisory Center (VAAC) responsible to provide ash warnings to the International Civil Aviation  
64 Organization (ICAO) across the Pacific Northwest (Sennert, 2019). In addition, KVERT and SVERT issued red  
65 warnings for aviation. As a result, nearly 40 flights were re-routed to avoid volcanic ash clouds.

66 Firstov et al., (2020) analyzed Infrasound Signal (IS) from ground stations in Kamchatka and found a total of 11  
67 explosive episodes (see Fig.1a). The first 8 episodes were followed by a continuous episode (9) which lasted for 3.5  
68 h. Based on IS analysis, episodes are separated into magma fragmentation/ non-stationary processes and vent



69 outflow (1,2,3,7,9 and 10) of ash-gas into the atmosphere. They were used to derive a minimal eruption tephra  
70 volume of  $0.1 \text{ km}^3$  allowing to categorize the eruption as Volcanic Explosivity Index (VEI) 4 (Firstov et al., 2020).  
71 Fig1b shows cloud top temperature ( $11 \mu\text{m}$ ) and associated cloud top heights derived from Himawari-8 geostationary  
72 satellite compared with IS data shown in Fig.1a. The eruption started at around 18:00 UTC on 21 June 2019  
73 followed by at least 8 discrete “bursts” (eruptions) and continuous emissions. A further two discrete pulses occurred  
74 later. The IS analysis coincides very well with the Himawari-8 observations where each IS corresponds to the  
75 release of volcanic cloud into the atmosphere. Muser et al. (2020) used one-dimensional volcanic plume models  
76 (Mastin, 2007; Folch et al., 2016) to invert the mass eruption rate of ash and initialize the ICON-ART (Zängl et al.,  
77 2015) dispersion model to investigate the complex aerosol, dynamical and radiative processes governing the plume  
78 evolution. More simplistic initialization approach with the dispersion model NAME (Beckett et al., 2020) and the  
79 aerosol-chemistry-climate model WACCM (Mills et al., 2016) were performed during the VolRes activities shortly  
80 after the eruption to assess the early dispersion of the plume.

81 As part of the scientific response to the eruption, the Volcano Response (Volres) initiative triggered an initial  
82 dialogue among the science community. VolRes is an international working group, within the Stratospheric Sulfur  
83 and its Role in Climate (SSiRC) to establish co-operation and community planning, for the next large-magnitude  
84 eruption, aligned also to the NASA initiative for US-based volcano response plan (Carn et al., 2021). The SSiRC  
85 initiative is itself an activity within the SPARC project of the World Climate Research Program (WCRP). Since its  
86 inception in 2015, VolRes consist of more than 250 scientists worldwide, from a diverse range of both model and  
87 observational experts, aiming to contribute from sharing and discussion of information related to the atmospheric  
88 impacts of volcanoes. Discussion and sharing to the mailing list is maintained through an archive and Wiki page,  
89 structured by eruption since 2018 (<https://wiki.earthdata.nasa.gov/display/volres<sup>2</sup>>).

90 The discussions on the VolRes forum have mostly been focused towards: i) establishing initial estimates of the  
91 emitted  $\text{SO}_2$  and ash, and injection heights estimates from multiple satellite observation platforms; ii) the expected  
92 impacts on stratospheric aerosol loadings; iii) factors to consider in modelling the aerosol cloud, towards then  
93 projecting radiative and climate effects; and iv) common related findings after other similar eruptions. Several cross-  
94 institutional co-operations resulted from the VolRes activity, which also motivated the Raikoke ACP/AMT/GMD  
95 inter-journal special issue “Satellite observations, in situ measurements and model simulations of the 2019 Raikoke  
96 eruption “. The Raikoke special issue includes a series of publications (Muser et al., 2020; Kloss et al., 2021;  
97 Vaughan et al., 2021; de Leeuw et al., 2021; Horváth et al., 2021a,b; Gorkavyi et al., 2021; Inness et al., 2022;  
98 Mingari et al., 2022; Osborne et al., 2022; Bruckert et al., 2022; Capponi et al., 2022; Cai et al., 2022; Harvey et al.,  
99 2022; Knepp et al., 2022; Prata et al., 2022; Petracca et al., 2022) focusing on the atmospheric impacts of this  
100 eruption using satellite Low Earth Orbiting/Geostationary nadir and limb observations from UV-Visible to far IR,  
101 model simulations, airborne measurements and ground-based lidar observations.

102 The goals of this paper is to:

- 103 • Describe the activities undertaken by the Volcano Response group (VolRes,  
104 <https://wiki.earthdata.nasa.gov/display/volres/Volcano+Response>) at the time of the 2019 Raikoke eruption. A



- 105 chronology of these activities is provided in Table 2.
- 106 • Give an overview of the early estimates of the mass of SO<sub>2</sub> emitted as well as the associated radiative forcing
- 107 and temperature response inferred quickly after the eruption.
- 108 • Discuss how revised estimates of SO<sub>2</sub> mass and plume heights as well as radiative forcing estimates differ from
- 109 the rapid assessment made a week after the eruption.
- 110 • Summarize the findings of the Raikoke special issue and highlight the remaining science questions as well as
- 111 the challenges associated with rapid response to volcanic eruptions in the context of atmospheric impacts.

## 112 2. Satellite Datasets

### 113 HIMAWARI-8

114 Himwari-8 is a spacecraft developed and operated by the Japanese Meteorological Organization (JAXA). The

115 primary instrument aboard Himawari 8 is the Advanced Himawari Imager (AHI), a 16 multi-channel spectral

116 imager to capture visible light and infrared images of the Asia-Pacific region at 500m horizontal resolution and

117 every 10 minutes. AHI is used to derived the cloud-top temperature and associated cloud top height associated with

118 the Raikoke eruption.

### 119 TROPOMI

120 The TROPospheric Monitoring Instrument (TROPOMI), on board the Sentinel-5 Precursor satellite provides

121 atmospheric composition measurements (Veefkind et al., 2012) at high spatial resolution of 3.5 x 5.5 km<sup>2</sup>.

122 TROPOMI is a hyperspectral sounder with different spectral bands from the ultraviolet (UV) to the short-wave

123 infrared. TROPOMI provides nearly global coverage in one day at 1.30 pm local time. For a rapid assessment of the

124 total emitted SO<sub>2</sub> mass, the operational SO<sub>2</sub> product (Theys et al., 2017) was used. A refined analysis was then

125 performed with the scientific SO<sub>2</sub> layer height and vertical column joint retrieval of Theys et al.(2022)

### 126 IASI

127 The Infrared Atmospheric Sounding Interferometer (IASI) is the high spectral resolution infrared sounder onboard

128 the operational Metop A-B-C platforms. With a morning and evening overpass (around 9:30 AM and PM),

129 combined with a large swath, the instrument samples the entire globe twice a day. Its footprint is a 12km diameter

130 circle at nadir viewing angles, gradually increasing to a 20 km x 39 km ellipse at the far end of its swath. The SO<sub>2</sub>

131 product that was used for rapid assessment is the one detailed in Clarisse et al. (2014). The retrieval algorithm

132 consists of two steps. First a so-called Z function that is estimated for each observed spectrum, using a set of

133 derivatives (Jacobians) with respect to the SO<sub>2</sub> partial columns at varying altitudes. The altitude at which Z function

134 reaches is maximum is the retrieved SO<sub>2</sub> height. In a second step, the estimated SO<sub>2</sub> height is used to constrain the

135 IASI SO<sub>2</sub> column retrieval. Note that the entire retrieval uses the 7.3 μm absorption band of SO<sub>2</sub>, which is less

136 affected by ash than the 8.6 μm band. While the altitude algorithm has a general accuracy better than 2 km, it is

137 known to underestimate the SO<sub>2</sub> altitude for high SO<sub>2</sub> columns. For the refined analysis discussed below, a new

138 experimental product was used that deals better with saturation issues.



139 **Aqua/AIRS**

140 The atmospheric Infrared Radiation Sounder (AIRS) instrument is on board the NASA polar-orbiting Aqua satellite  
141 at an altitude of about 705 km above the Earth surface with an Equatorial crossing time at 1.30am/pm local time  
142 (Chahine et al., 2005; Prata & Bernardo, 2007). AIRS provides nearly continuous measurement coverage during  
143 14.5 orbits per day and a 95% global daily coverage with a swath of 1650 km and spectral resolution of 13.5 km x  
144 13.5 km at nadir (Tournigand et al., 2020). We use the version 7.0 AIRS level 2 Support Retrieval product, and the  
145 results are averaged into 1° x 1° grid cells in this analysis. The brightness temperature difference (less than -6 K) is  
146 used as a proxy of SO<sub>2</sub> released from volcanoes.

147 **CALIPSO/CALIOP**

148 The Cloud-Aerosol Lidar with Orthogonal Polarization (CALIOP), on board the Cloud-Aerosol Lidar and Infrared  
149 Pathfinder Satellite Observations (CALIPSO) platform, has been providing aerosol vertical profile measurements of  
150 the Earth's atmosphere on a global scale since June 2006 (Winker et al., 2010). We use the version 4.21 CALIOP  
151 level 2 Aerosol layer and Cloud layer products and only quality screened samples are used in the analysis. Aerosol  
152 layers with Cloud Aerosol Discrimination (CAD) score less than -100 or greater than -20 are rejected to avoid low  
153 confidence in cloud-air discrimination. Aerosol layers with the extinction Quality Control (QC) flag that are not  
154 equal to 0, 1, 16, and 18 are rejected to remove low confidence extinction retrievals, and aerosol extinction samples  
155 with the extinction uncertainty equal to 99.99 km<sup>-1</sup> and all samples at lower altitudes in the profile are rejected to  
156 remove unreliable extinctions (Winker et al., 2013).

157 Firstov et al., (2020) analyzed Infrasound Signal (IS) from ground stations in Kamchatka and found a total of 11  
158 explosive episodes (see Fig. 1a). The first 8 episodes were followed by a continuous episode (9) which lasted for 3.5  
159 h. Based on IS analysis, episodes are separated into magma fragmentation/ non-stationary processes and vent  
160 outflow (1,2,3,7,9 and 10) of ash-gas into the atmosphere. They were used to derive a minimal eruption tephra  
161 volume of 0.1 km<sup>3</sup> allowing to categorize the eruption as Volcanic Explosivity Index (VEI) 4 (Firstov et al., 2020).  
162 Fig 1b shows cloud top temperature (11µm) and associated cloud top heights derived from Himawari-8 geostationary  
163 satellite compared with IS data shown in Fig. 1a. The eruption started at around 18:00 UTC on 21 June 2019  
164 followed by at least 8 discrete “bursts” (eruptions) and continuous emissions. A further two discrete pulses occurred  
165 later. The IS analysis coincides very well with the Himawari-8 observations where each IS corresponds to the  
166 release of volcanic cloud into the atmosphere. Muser et al. (2020) used one-dimensional volcanic plume models  
167 (Mastin, 2007; Folch et al., 2016) to invert the mass eruption rate of ash and initialize the ICON-ART dispersion  
168 model to investigate the complex aerosol, dynamical and radiative processes governing the plume evolution. More  
169 simplistic initialization approach with the dispersion model NAME and the aerosol-chemistry-climate model  
170 WACCM were performed during the VolRes activities shortly after the eruption to assess the early dispersion of the  
171 plume.

172

173 **4. Early reports of injection parameters one week after the eruption**



174 One of the main activities of a satellite sub-group formed within the framework of VolRes was to derive eruption  
175 parameters characterizing SO<sub>2</sub> emissions (e.g. mass, bulk height, injection profiles) so that modelers would run  
176 numerical simulations to understand the potential hazards and climate impacts of this eruption. The basic approach  
177 to estimate the total mass of SO<sub>2</sub> is similar for each satellite-based sensor. First, the process involves retrieving the  
178 Vertical Column Density (VCD, measured in molecules cm<sup>-2</sup> or g m<sup>-2</sup> or Dobson units) in each pixel affected by  
179 SO<sub>2</sub>, followed by multiplying by the area of the pixels and integrating all the pixels to calculate the total SO<sub>2</sub>  
180 loadings. However, there are limitations to this method. Indeed, narrow swath width sensors, timing of the polar  
181 orbit and, in the case of the geostationary sensors, extreme viewing geometry (high satellite zenith angles) and  
182 movement out of the field of view will introduce errors (likely underestimations) of the total mass. There are also  
183 many assumptions used by the various algorithms that if not valid will introduce errors, as will discussed hereunder.  
184 When the Vertical Column Densities (VCDs) are large (>500 DU) most algorithms have difficulty estimating the  
185 VCD correctly (Hyman and Pavolonis, 2020; Prata et al. 2021). Figure 2 shows the time evolution of the total SO<sub>2</sub>  
186 mass during and after the Raikoke eruption from multiple sensors. The measurements discussed here all assume SO<sub>2</sub>  
187 in the UTLS (7–12 km). The SO<sub>2</sub> retrieved from Himawari-8 peaks near 1.5 Tg nearly 48h after the beginning of the  
188 eruption and follow similar temporal evolution than the one derived from LEO. Given the likelihood that most  
189 satellites underestimated the SO<sub>2</sub> mass, we chose at that time the maximum value from Himawari and the upper  
190 limits of the other sensors yielding a 1.5+/-0.2 Tg estimation. IASI, TROPOMI and CALIPSO data suggested that  
191 SO<sub>2</sub> was injected within a large altitude range from the ground up to well in the stratosphere (at least 15 km). In  
192 addition to a total mass of SO<sub>2</sub> (of 1.5 Tg), the VolRes team also issued a provisional vertical distribution of the  
193 emitted SO<sub>2</sub> mass that could be used by dispersion and climate modelers. To do so, IASI SO<sub>2</sub> height measurements  
194 on the 22<sup>nd</sup> June 2019 were used. The mass-altitude indicated that most SO<sub>2</sub> was released between 8-12 km with a  
195 secondary peak around 14-15 km. Scaled to the proposed 1.5 Tg, the distribution is shown in Figure 3 and is referred  
196 to as the ‘VolRes profile’ (blue line; also see Table 1). For TROPOMI, and other LEOs, the plume can be partly  
197 covered by a given orbit but using the multiple orbits of one day and the fact that they generally overlap most of the  
198 plume is covered. To avoid double counting, the data of one full day are usually averaged on a regular latitude-  
199 longitude grid, before the actual emitted SO<sub>2</sub> mass is calculated. An important source of error is the vertical  
200 distribution of SO<sub>2</sub>. In Fig.2, the retrieved SO<sub>2</sub> mass from TROPOMI was calculated by assuming a bulk plume  
201 height of 15 km (all plume heights given above sea level unless specified). This assumption can introduce errors  
202 (underestimation) in particular for clear-sky scenes and if the SO<sub>2</sub> is in the (lower) troposphere, typically below  
203 7km, see e.g., Fig 1 of Theys et al. (2013). TROPOMI has less limitations in retrieving very large SO<sub>2</sub> columns  
204 (>500 DU) because in that case the spectral range used (360-390nm) is weakly affected by saturation due to non-  
205 linear SO<sub>2</sub> absorption (Bobrowski et al., 2010). The main problem is the presence of aerosols which are not  
206 explicitly treated in the retrievals (Theys et al., 2017). For ash, the photons cannot penetrate deep in the volcanic  
207 cloud (only the cloud top layer is sensed) and this leads to a strong underestimation of the mass of SO<sub>2</sub> (by a factor  
208 of 5 or so).

## 209 **5. Revision and improvements of injection parameters.**



210 While the accuracy of the IASI SO<sub>2</sub> height retrievals is typically better than 2km, it became clear however that the  
211 VolRes profile was peaking too low in the atmosphere (e.g., de Leeuw et al., 2021). The main reason for this is related  
212 to the SO<sub>2</sub> Jacobians used in the retrieval. These are precalculated for relatively low SO<sub>2</sub> VCDs and are not directly  
213 applicable to saturated plumes, as encountered during the Raikoke eruption. Refinement of the IASI algorithm to  
214 better account for this dependence on the SO<sub>2</sub> loadings has led to SO<sub>2</sub> injection profile with a maximum SO<sub>2</sub> peaking  
215 at ~14-15 km (see Figure 3) and a slightly lower total mass of ~1.3 Tg SO<sub>2</sub> (even though total mass estimates for the  
216 days after reach again 1.5 Tg and higher).

217 As an alternative to IASI, ultraviolet observations from the TROPOMI nadir sensor have been used to estimate the  
218 SO<sub>2</sub> injection profile (Table 1). Conceptually, the retrieval algorithm is like the IASI scheme. It relies on an iterative  
219 approach making use of a SO<sub>2</sub> optical depth look-up-table, where both SO<sub>2</sub> height and vertical column are retrieved  
220 jointly (Theys et al., 2021). The accuracy of the retrieved SO<sub>2</sub> heights is of 1-2 km, except when coincident with fresh  
221 and optically thick ash plumes for which the estimated heights can be strongly biased low. Because of this, the first  
222 reliable profile from TROPOMI which covers the full plume, is for the 24 June 2019. The maximum SO<sub>2</sub> height is  
223 found at ~11-12 km (Figure 3) and the total mass derived is of ~1.2 Tg SO<sub>2</sub>. However, the total mass is likely  
224 underestimated because only the pixels with confident SO<sub>2</sub> height retrievals are considered (typically for SO<sub>2</sub> columns  
225 > 5DU). Selected examples of retrieved SO<sub>2</sub> heights from the two instruments are illustrated in Figure 4.

226 Although the estimated SO<sub>2</sub> mass from IASI and TROPOMI agree well, the estimated SO<sub>2</sub> profiles show rather  
227 inconsistent results with a discrepancy of about 3km for the SO<sub>2</sub> bulk height. It should be emphasized that SO<sub>2</sub> height  
228 retrieval from nadir sensors is challenging in general but for Raikoke in particular. The retrievals and their  
229 interpretation might also suffer from different aspects. For instance, the UTLS was characterized by isothermal  
230 temperature profiles, which can lead to errors on the IASI height estimates. In addition, the measurement sensitivity  
231 is different in the ultraviolet than in the thermal infrared and depends on the way the photons interact with the volcanic  
232 cloud (and the constituents other than SO<sub>2</sub>). In this respect, the retrieved SO<sub>2</sub> heights must be considered as effective  
233 heights. Moreover, few CALIOP observations were available (see Section 6) for evaluating the results for the early  
234 stage of the eruption.

235 Despite these challenges, our injection profiles estimates are not in contradiction with results found in the literature:

- 236 • Kloss et al. (2021) reported a 14 km altitude plume height based on an early OMPS aerosol extinction profile,  
237 on 22 June 2019.
- 238 • Muser et al. (2020) derived typical altitudes of 8-14 km from MODIS and VIIRS cloud top height retrievals.
- 239 • By slightly adapting (assuming higher injection heights) the VolRes profile, de Leeuw et al. (2021) found  
240 the best match between modeled and TROPOMI SO<sub>2</sub> columns for an injection profile with most of SO<sub>2</sub>  
241 between 11 and 14 km.
- 242 • Hedelt et al. (2019) reported SO<sub>2</sub> heights similar to the TROPOMI results shown here, i.e., with the bulk  
243 height below 13km.





- 244 • SO<sub>2</sub> height retrievals from the Cross-track Infrared Sounder (CrIS) instrument (Hyman & Pavolonis, 2020)  
245 are consistent with plume heights as high as 14-17 km in the plume center, but also show that most of the  
246 SO<sub>2</sub> mass was emitted under 13 km.
- 247 • Geometric estimation of Raikoke ash column height suggests injection mainly between 5 and 14 km and an  
248 overshooting cloud up to 17 km (Horváth et al., 2021b).
- 249 • MLS data for 23-27 June indicates SO<sub>2</sub> plumes at 11 to 18 km with maximum columns observed around 14  
250 km (Gorkavyi et al., 2021).
- 251 • Using a Langragian transport model combined with TROPOMI and AIRS, Cai et al. (2022) reconstruct an  
252 emission profile with a peak at 11 km with a large spread from 6 to 14 km.
- 253 • Prata et al. (2022) found ash clouds at a maximum height of 14.2 km (median height of  $10.7 \pm 1.2$  km) during  
254 the main explosive phase.

## 255 **6. New plume injection analysis derived from CALIPSO and AIRS**

256 CALIPSO observations were made publicly available within 24-48 h after the beginning of the eruption allowing  
257 accurate early estimates of the height of downwind plume sections. However, due to the narrow swath of the lidar (a  
258 few hundred meters) and consequently low horizontal resolution, they may not completely represent the entire  
259 plume vertical distribution. Nevertheless, an overpass of the CALIPSO lidar across the plume on 22 June 2019 at  
260 2.15 am, ~600 km east from the volcano within an SO<sub>2</sub> cloud observed by OMPS show volcanic layers between 9-  
261 13.5 km (Prata et al., 2021). A second overpass the next day depicts another volcanic layer between 15-16 km.  
262 Those observations were used to validate SO<sub>2</sub> emission profiles provided to the community a week after the  
263 eruption. Here, we give a more comprehensive analysis of the plume injection height using a combination of quasi-  
264 collocated (less than 1h apart) SO<sub>2</sub> observations from AIRS and detected volcanic layers from CALIOP during the  
265 first two weeks after the eruption. The brightness temperature difference ( $1361.44-1433.06$  cm<sup>-1</sup>) is used as a proxy  
266 of SO<sub>2</sub> released from volcanoes to identify CALIOP data within the SO<sub>2</sub> plume.

267 We combined SO<sub>2</sub> information from AIRS quasi-collocated observations from CALIOP to further investigate plume  
268 injection heights after the Raikoke eruption assuming that SO<sub>2</sub> and volcanic aerosols remained collocated in space  
269 and time during the first 10 days after the eruption. Figure 5 shows a map of SO<sub>2</sub> derived from AIRS together with  
270 CALIOP orbit tracks (red). The corresponding cloud and aerosol level 2 V4.2 products are plotted along with BTD  
271 extracted along the orbit. All corresponding layers (clouds and aerosols) associated with negative BTD (<6 K),  
272 indicating the presence of SO<sub>2</sub> in the atmospheric column, have been further analyzed to distinguish the volcanic  
273 plume. The distinction is based on the diagram of depolarization and color ratio shown in panel d. Figure 5 shows  
274 that CALIOP intersected the plume along two orbit tracks on 25 June. The first being along the 17h53 UTC orbit  
275 near 60°N and at two occasions between 55°N-65°N along the second orbit near 14h36 UTC. The first intersection  
276 shows the plume near 9-11 km with weak particulate DePolarization Ratio (DPR) (DPR < 0.2) and particulate  
277 CoLor Ratio (CLR) near 0.5. DPR values suggest a mixture of ash and sulfate aerosols. However, the second  
278 intersection of the plume shows higher DPR near 0.3 and the same CLR than the first indicating a higher fraction of  
279 ash particles resulting in increased DPR values. During those observations, two distinct plumes are visible between





280 the northern intersection near 11-13 km (green color on diagrams) and a piece at higher altitude (13-15 km) further  
281 south (<60°N). We visually inspected all CALIOP observations (day and night) between 06/22 and 07/06 following  
282 the same approach and used plume identification criterion when  $DPR < 0.4$  and  $CLR < 0.7$  and altitude  $> 5$  km to  
283 remove tropospheric aerosols and ice clouds. Because of the enhanced noise of the daytime observations, we chose  
284 to focus this analysis on nighttime data only. Figure 6 shows the daily observations of the Raikoke plume since the  
285 eruption and during the following two weeks. We note that the plume was observed by CALIOP from 8 km to 17  
286 km. The cumulative Probability Density Function (pdf) suggests two main peaks, one near 10-11 km and another  
287 smoother peak near 13-15 km. The overall aerosol vertical distribution is consistent with the distribution of  $SO_2$   
288 profiles derived with different approaches and instruments just after the eruption (Fig.3). However, the pdf does not  
289 suggest a pronounced peak at a given altitude but rather a flatter distribution as opposed to what is shown in Figure  
290 3. The pdf does not account for or is not weighted by the aerosol loading which may explain why we do not see a  
291 pronounced peak as for the  $SO_2$  profiles derived from IASI and TROPOMI. In addition,  $SO_2$  and volcanic aerosol  
292 layers are assumed to be collocated but it may not always be the case.

### 293 **7. Rapid projections of the aerosol forcing and the global mean surface temperature response.**

294 In the previous sections, we discussed in detail the methods used to derive injection parameters ( $SO_2$  total mass,  
295 plume heights and  $SO_2$  distribution) which served as input to estimate the radiative and surface temperature  
296 responses from the eruption in this section. Key metrics characterizing the climate effects of volcanic eruptions are  
297 the peak global mean mid-visible SAOD, the global mean net radiative forcing and the global mean surface  
298 temperature change. One motivation of the VolRes initiative is to provide an estimated magnitude for each of these  
299 metrics. In the case of a large-magnitude eruption, these initial indicators of the scale of the climate response would  
300 then help to determine whether resources should be directed towards additional measurement campaign and the  
301 forcing datasets enable the community to run seasonal and decadal forecasts (Müller and Smith, 2018).

302 The first estimates of the injected  $SO_2$  mass and height became available 24-48 hours after the 2019 Raikoke  
303 eruption, followed one week later by an estimate of global mean peak SAOD (7.1), radiative forcing (7.2) and  
304 surface temperature (7.3). This section discusses: i) how these estimates were made; ii) how they compared to  
305 observations; and iii) ongoing improvements to the protocol for rapid projection of volcanic forcing and climate  
306 impact.

#### 307 **7.1 Model simulations of aerosol optical properties**

308 We first made projections for SAOD on 25 June 2019 using EVA\_H (Aubry et al., 2020), a simple volcanic aerosol  
309 model based on inputs of the mass of volcanic  $SO_2$  injected, its injection height, and the latitude of an eruption. The  
310 first estimates made following Raikoke used a range of injection heights between 10-20 km, and a range of the mass  
311 of  $SO_2$  of 1-2 Tg of  $SO_2$ , on the basis of first estimates of 14 km and 1.5 Tg of  $SO_2$  that initially circulated on the  
312 VolRes mailing list (personal communication from Taha Ghassan and Lieven Clarisse). The corresponding  
313 simulated range in peak Northern Hemisphere (25°N-90°N, NH) monthly-mean SAOD at 525nm (SAOD<sub>525</sub>) was  
314 0.015-0.023 (Figure 7). This range was obtained using Monte Carlo methods, i.e. EVA\_H was run thousands of



315 times randomly resampling the range of injection height and mass. The negligible computational cost of simple  
316 models like EVA\_H is a key advantage for providing estimate of the volcanic SAOD perturbation and its  
317 uncertainties as soon as measurements of the SO<sub>2</sub> mass and its injection height become available. The SAOD  
318 perturbation was projected to be largely confined to 25-90°N (Figure 8). SAOD perturbations observed in the tropics  
319 and Southern Hemisphere over 2019-2020 (Figure 8) are primarily driven by stratospheric emissions from the  
320 Ulawun 2019 eruptions and the Australian 2019-2020 wildfires (Kloss et al., 2021).

321 Following the communication of the initial VolRes SO<sub>2</sub> profile (Figure 3) through the VolRes mailing list, EVA\_H  
322 peak NH monthly-mean SAOD<sub>525</sub> estimate for Raikoke were revised to an even smaller value of 0.014. Compared to  
323 observations from GloSSAC (v2.1) (Kovilakam et al., 2020), this value was largely underestimated as GloSSAC NH  
324 monthly-mean SAOD<sub>525</sub> peaks at 0.025 (Figure 7, with GloSSAC in excellent agreement with observational values  
325 from Kloss et al., 2021) using OMPS-limb data. The new IASI June 22 profile presented in Figure 3 results in a  
326 higher peak NH monthly-mean SAOD<sub>525</sub> of 0.0175, with the higher proportion of stratospheric SO<sub>2</sub> in the new  
327 profile more than compensating for the total mass decreasing from 1.5 to 1.29 (average of the two IASI profiles) Tg  
328 of SO<sub>2</sub>. Although the new SO<sub>2</sub> emission profile improves agreement with observations, the estimated SAOD<sub>525</sub>  
329 value is still a substantial underestimate. Furthermore, the characteristic rise and decay timescales of the SAOD<sub>525</sub>  
330 perturbation are also overestimated by EVA\_H (Figure 7). These mismatches are caused by the constant timescale  
331 EVA\_H uses for SO<sub>2</sub> to sulfate aerosol conversion, which is biased towards an 8-month value adequate for the  
332 Pinatubo 1991 eruption (Aubry et al, 2020). If we decrease the value of this timescale by 66% to 2.8 month in  
333 EVA\_H, the NH peak SAOD value as well as the characteristic rise and decay timescale of the SAOD perturbation  
334 are in excellent agreement with observations for the 2019 Raikoke eruption (Figure 7). The fact that this model  
335 timescale is independent of the eruption characteristic is an already identified weakness of EVA\_H that will be  
336 addressed in future developments (Aubry et al., 2020). This timescale has indeed been shown to depend on the  
337 volcanic SO<sub>2</sub> mass (e.g. McKeen et al., 1984; Carn et al, 2016), injection altitude and latitude (e.g. Carn et al, 2016,  
338 Marshall et al. 2019) as well as co-emission of water vapor (Legrande et al., 2016) and volcanic ash (Zhu et al.,  
339 2022).

## 340 **7.2 Projection for global mean volcanic forcing**

341 On the same day that SAOD projections were initially provided, Piers Forster independently suggested via the  
342 VolRes mailing list (Forster, personal communication) that the global annual-mean net radiative forcing would be at  
343 most -0.2 W m<sup>-2</sup> based on a scaling between the estimated SO<sub>2</sub> mass of 1.5 Tg SO<sub>2</sub> for 2019 Raikoke and the  
344 estimated 15-20 Tg SO<sub>2</sub> for the 1991 Mt. Pinatubo eruption, which resulted in a global annual-mean forcing of -3.2  
345 W/m<sup>2</sup> in 1992. This projection was a back-of-the-envelope calculation using simple proportionality arguments and it  
346 did not rely on any SAOD estimates. A monthly global mean peak shortwave forcing with a range from -0.16 to  
347 -0.11 W/m<sup>2</sup> was derived from SAGE III observations (Kloss et al., 2021). The corresponding annual mean net  
348 forcing is expected to be much smaller because of the difference between the peak monthly NH mean SAOD and its  
349 average value over the first post-eruption year (Figure 7), as well as the fact that longwave stratospheric volcanic



350 aerosol forcing can offset as much as half of the shortwave forcing (Schmidt et al. 2018). Altogether, the educated  
351 guess made for global annual mean radiative forcing was thus likely overestimated.

### 352 **7.3 Projection of the global mean surface temperature response**

353 Last, as part of the eruption response, one day after the first global annual-mean radiative forcing estimate of 0.2 W  
354 m<sup>-2</sup> was made, we estimated that the peak global annual-mean surface temperature change would be -0.02 K (Figure  
355 9). We obtained this estimate using FaIR, a simple climate model (Smith et al., 2018). Like EVA\_H, FaIR has a  
356 negligible computational cost enabling rapid estimates of global-mean surface temperature change following an  
357 eruption and facilitating uncertainty estimation, although the latter was not done for the 2019 Raikoke eruption. The  
358 model-projected surface temperature response cannot be compared to measurements owing to difficulties in  
359 disentangling such a small forced temperature response from temperature variations related to natural variability.

## 360 **8. Discussions**

361 The Raikoke eruption ended a period without moderate volcanic eruptions in the Northern Hemisphere since Nabro  
362 in 2011 (Bourassa et al., 2013, Fairlie et al., 2014; Sawamura et al., 2012) which injected 1.5-2 Tg of SO<sub>2</sub> partially  
363 distributed between the troposphere and stratosphere. Following the Nabro eruption, the role deep convection during  
364 the Summer Asian Monsoon was evoked to explain an apparent ascent of the plume (Bourassa et al., 2013) debated  
365 by others (Fromm et al., 2013, Vernier et al., 2013) based on initial observations of injection heights. The substantial  
366 debate provoked by this eruption clearly demonstrated the complexity of assessing accurately SO<sub>2</sub> injection heights  
367 and their partition relative to the tropopause. The VolRes initiative substantially helps fill those gaps by providing a  
368 coordinated structure to derive injection parameters after the Raikoke eruption. Multiple sensors were used to assess  
369 the total SO<sub>2</sub> mass and its distribution just one week after the eruption (Fig.3). However, the lack of vertically  
370 resolved SO<sub>2</sub> information remains a limitation to accurately assess SO<sub>2</sub> plume distribution and the revised estimates  
371 proposed here remain with a 2 km uncertainty regarding the exact position of the plume peak while the initial 1.5 Tg  
372 SO<sub>2</sub> mass estimate might be slightly overestimated. Advances in measuring SO<sub>2</sub> with lidar observations may fill  
373 those gaps in the future.

374 The VolRes team provided eruptive parameters within a week after the eruption that strongly helped modelers to  
375 estimate climate response of the Raikoke eruption. The use of simple models like EVA\_H and FaIR to project the  
376 climate response to an eruption in almost near real-time is a powerful way to generate first-order estimates of the  
377 perturbations to SAOD, and surface temperatures. Unlike simple proportionality arguments based on the Pinatubo  
378 1991 eruption, these models can estimate the time (and spatial, for EVA\_H) evolution of the response variable, and  
379 they account for complexities such as the dependency of SAOD on the SO<sub>2</sub> injection latitude and height. Their  
380 computationally inexpensive nature also enables a comprehensive quantification of uncertainties related to eruption  
381 source parameters, which are often poorly constrained in the days-months following an eruption as highlighted by  
382 this special issue, as well as uncertainties on parameters of these empirical models, such as the SO<sub>2</sub>-aerosol  
383 conversion timescale in EVA\_H (Figure 7).



384 One limitation of the application of these models following the Raikoke 2019 event is that they were not applied in  
385 concordance, i.e. FaIR was run using an expert guess for the radiative forcing instead of values derived from  
386 EVA\_H's SAOD estimates (see section 7.2 and 7.3). Following the Raikoke 2019 VolRes response, we combined  
387 the simple models EVA\_H (for aerosol forcing) and FaIR (for surface temperature response). To do so, we apply  
388 simple linear (Schmidt et al., 2018) or exponential (Marshall et al., 2020) relationships to derive the global mean  
389 radiative forcing (FaIR's key input) from the global mean SAOD (one of EVA\_H's outputs). EVA\_H, SAOD-  
390 radiative forcing scalings, and FaIR were for example applied in concordance to estimate the climate impacts from  
391 the sulfate aerosols of the January 2022 Hunga Tonga-Hunga Ha'apai eruption. These models have been combined  
392 into a single dedicated webtool called Volc2Clim (Schmidt et al., 2023), publicly available at  
393 <https://volc2clim.bgs.ac.uk/>. Applied to Raikoke 2019 using the new injection profile (Figure 3) and revised SO<sub>2</sub> to  
394 sulfate aerosol conversion timescale, the beta version of Volc2Clim projected peak global mean of 0.008, -0.17  
395 W/m<sup>2</sup> and -0.028 K for monthly mean SAOD, monthly mean radiative forcing and annual mean temperature  
396 anomaly. In addition to key metrics discussed in this section such as global mean SAOD, radiative forcing and  
397 surface temperature, aerosol optical properties field (dependent on latitude, altitude and wavelength) are outputted  
398 by Volc2Clim for use in climate models that do not have an interactive stratospheric aerosol scheme. With a webtool  
399 for rapid estimation of the global climate response during an eruptive crisis, we hope to support communication  
400 amongst the scientific community (including VolRes), with authorities and with the public, which in turn will help  
401 to mitigate potential consequences arising from the climate effects of an eruption.

402 Although Volc2Clim offers new perspectives for rapid response and communication following volcanic eruptions,  
403 the simplified nature of the models at its core currently do not allow projections of effects related to co-emission of  
404 species such as water vapor or halogen in volcanic plumes, or PyroCumulonimbus (PyroCbs) plumes. Before and  
405 after the Raikoke eruption, three significant events affected stratospheric aerosols. Indeed, SO<sub>2</sub> injected from the  
406 June an August 2019 Ulawun eruptions and smoke from PyroCbs in Canada made the Raikoke eruption even more  
407 challenging to understand. The PyroCbs in Canada produced smoke in the UTLS one week before the eruption, but  
408 the transport patterns of smoke and volcanic aerosols have been distinct (Osborne et al., 2022) and the likelihood for  
409 both plumes to mix is relatively small. The Ulawun eruption injected SO<sub>2</sub> which remained relatively confined in the  
410 Southern Hemisphere, but we cannot rule out that both plumes got mixed in the tropics (Kloss et al., 2021). The  
411 relatively small amount of SO<sub>2</sub> injected by Ulawun (< 0.1 Tg) was not considered in the estimates provided in this  
412 paper. Another interesting feature observed after the Raikoke eruption was the formation of a distinct plume which  
413 rose into the stratosphere. The plume formed a vortex circulation which remained coherent for several weeks  
414 (Gorkavyi et al., 2021) rising in the stratosphere of 10 km over the course of 2-3 months. While this plume shared  
415 similar optical properties to smoke, Knepp et al. (2022) concluded that this layer was mostly composed of large  
416 sulfuric acid droplets but did not refute the possible presence of a fine ash component. More recently (Khaykin et al,  
417 2023) found that 24% of the total SO<sub>2</sub> mass was contained in the volcanic vortex with a confined anticyclonic  
418 circulation detected by wind doppler lidar from Aeolus. A warm anomaly of 1 K was also evident GPS RO Cosmic  
419 data demonstrating that the heating of the plume was indeed responsible for its internal circulation and maintenance.  
420 Moreover, the properties of the plume observed by CALIOP showed the persistence of ash that likely induced



421 internal heating in the plume consistent with earlier observations of volcanic clouds after the Kelud and Puyehue-  
422 Cordon eruptions (Jensen et al., 2018; Vernier et al., 2013, 2016). While the presence of fine ash in the Raikoke  
423 could likely explained the maintenance of the vortex as observed after PyroCbs events but with a much faster ascent  
424 rate, the interplay between ash and sulfate and influence on radiative calculations is still not understood (Vernier et  
425 al., 2016; Stenchikov et al., 2021; Zhu et al., 2020). In addition, we cannot fully rule out that remnants of smoke  
426 from the PyroCbs in Canada one week before the eruption could have played a role in the transport of the plume.  
427 The increased lifetime of this plume may have produced a larger climate impact than expected since this effect is not  
428 included in the simple model provided in this paper (Figure 8).

429 Finally, the recent eruption of Hunga Tonga Hunga Ha'apai demonstrated that sub-marine eruption can inject  
430 significant amount of H<sub>2</sub>O in the stratosphere (Milan et al., 2022, Vogel et al., 2022; Sellitto et al., 2022) which is  
431 known to have opposite cooling climate effects than sulfate aerosol. The water vapor can reduce the lifetime of  
432 SO<sub>2</sub> by providing OH radicals and affect aerosol size distribution through condensational growth (Zhu et al., 2022).  
433 Such effects are not included in the simple climate estimates provided here and would limit its applicability in the  
434 case of HTHH if only the climate impacts of sulfate aerosols are considered.

## 435 **9. Conclusion**

436 VolRes is an international coordinated initiative to study the atmospheric impacts of volcanic eruptions, now  
437 involving more than 250 researchers worldwide. The 2019 Raikoke eruption triggered significant responses by the  
438 VolRes community through exchanges of information via the mailing list and the preparation of SO<sub>2</sub> profile  
439 recommendations for modelers made available a week after the eruption only. Our paper gives a brief overview of  
440 how the community responded to this volcanic eruption, which is documented extensively in the Raikoke special  
441 issue. We then described how early estimates of SO<sub>2</sub> emission and height, a fundamental parameter which dictates  
442 the plume lifetime and its impacts, were derived from satellite observations. These estimates were used by VolRes to  
443 calculate SAOD, radiative forcings and surface temperature changes as part of the initial eruption response. We  
444 revisited the initial SO<sub>2</sub> injection profiles by addressing saturation effects due to high SO<sub>2</sub> column density to  
445 improve plume injection heights. We highlight remaining challenges in accurately representing the vertical  
446 distribution for moderate- SO<sub>2</sub> explosive eruptions in the lowermost stratosphere due to limited vertical sensitivity of  
447 current satellite sensors (+/- 2 km accuracy) and low horizontal resolution of lidar observations. We found that using  
448 revisited SO<sub>2</sub> injection heights and reduced SO<sub>2</sub>-aerosol conversion timescale in a simple volcanic aerosol model  
449 (EVA\_H) improves SAOD estimates relative to available observations from the GloSSAC dataset. The protocol for  
450 fast estimation of aerosol optical properties, radiative forcing and surface temperature response to volcanic eruption  
451 has since been implemented in a seamless webtool (Volc2Clim, <https://volc2clim.bgs.ac.uk/>). The computationally  
452 inexpensive nature of the webtool makes it ideal for rapid assessment of the volcanic climate effect and for  
453 propagating large uncertainties that characterize early observations of volcanic clouds. Further development of the  
454 underlying simple models as well as continued use of complex models explicitly modelling aerosol chemistry,  
455 microphysics and transport remain critical given the complex nature of volcanic events. For example, the Raikoke  
456 eruption took place in connection with two eruptions of Ulawun in June and August 2019 and just after a PyroCb



457 event which transported smoke into the stratosphere which were not considered in our original or revised  
458 calculations. In addition, the recent HTHH eruption demonstrated that water vapor can also be injected into the  
459 stratosphere which can affect SO<sub>2</sub> and aerosol lifetime but also with a radiative forcing that is opposite to volcanic  
460 sulfate aerosols.

### 461 **Competing interests**

462 The contact author has declared that none of the authors has any competing interests.

### 463 **Acknowledgement.**

464 JPV and HC were supported by the NASA Roses program through the SAGE III Science Team (80NSSC21K1195)  
465 and Upper Atmosphere Composition Observations program (80NSSC21K1082). TJA was supported by a global  
466 mobility grant from the University of Exeter and a travel award from the Canada-UK foundation. ATP  
467 acknowledges funding from the Natural Environment Research Council (NERC) R4Ash project (NE/S003843/1).  
468 The Volc2Clim tool was kindly supported by the UK Earth System Modelling project, funded by the UKRI –  
469 Natural Environment Research Council (NERC) national capability grant number NE/N017951/1 and the Met  
470 Office, as well as NERC grants NE/S000887/1 (VOL-CLIM) and NE/S00436X/1 (V-PLUS). The GloSSAC data  
471 were obtained from the NASA Langley Research Center Atmospheric Sciences Data Center. The Volc2Clim  
472 webtool is available at <https://volc2clim.bgs.ac.uk/>, and the source code is available on GitHub at  
473 <https://github.com/cemac/volc2clim/>. The source code of the EVA\_H volcanic aerosol model is available on GitHub  
474 at [https://github.com/thomasaubry/EVA\\_H](https://github.com/thomasaubry/EVA_H). The source code of the FaIR climate model is available on Github at  
475 <https://github.com/OMS-NetZero/FAIR>.

476

### 477 **References:**

478  
479 Aubry, T. J., Toohey, M., Marshall, L., Schmidt, A., & Jellinek, A. M. (2020). A New Volcanic Stratospheric  
480 Sulfate Aerosol Forcing Emulator (EVA\_H): Comparison With Interactive Stratospheric Aerosol Models.  
481 *Journal of Geophysical Research: Atmospheres*, 125(3), e2019JD031303.  
482 <https://doi.org/https://doi.org/10.1029/2019JD031303>  
483  
484 Beckett, Frances M., et al. "Atmospheric dispersion modelling at the London VAAC: A review of developments  
485 since the 2010 eyjafjallajökull volcano ash cloud." *Atmosphere* 11.4 (2020): 352.  
486  
487 Bobrowski, N., Kern, C., Platt, U., Hörmann, C., & Wagner, T. (2010). Novel SO<sub>2</sub> spectral evaluation scheme using  
488 the 360–390 nm wavelength range. *Atmospheric Measurement Techniques*, 3(4), 879–891.  
489 <https://doi.org/10.5194/amt-3-879-2010>  
490



- 491 Bourassa, A. E., Robock, A., Randel, W. J., Deshler, T., Rieger, L. A., Lloyd, N. D., Llewellyn, E. J. (Ted), &  
492 Degenstein, D. A. (2012). Large Volcanic Aerosol Load in the Stratosphere Linked to Asian Monsoon  
493 Transport. *Science*, 337(6090), 78–81. <https://doi.org/10.1126/science.1219371>
- 494
- 495 Bruckert, J., Hoshyaripour, G. A., Horváth, Á., Muser, L. O., Prata, F. J., Hoose, C., and Vogel, B.: Online treatment  
496 of eruption dynamics improves the volcanic ash and SO<sub>2</sub> dispersion forecast: case of the 2019 Raikoke  
497 eruption, *Atmos. Chem. Phys.*, 22, 3535–3552, <https://doi.org/10.5194/acp-22-3535-2022>, 2022.
- 498
- 499 Cai, Z., Griessbach, S., & Hoffmann, L. (2022). Improved estimation of volcanic SO<sub>2</sub> injections from satellite  
500 retrievals and Lagrangian transport simulations: the 2019 Raikoke eruption. *Atmospheric Chemistry and*  
501 *Physics*, 22(10), 6787–6809. <https://doi.org/10.5194/acp-22-6787-2022>
- 502
- 503 Capponi, A., Harvey, N. J., Dacre, H. F., Beven, K., Saint, C., Wells, C., and James, M. R.: Refining an ensemble of  
504 volcanic ash forecasts using satellite retrievals: Raikoke 2019, *Atmos. Chem. Phys.*, 22, 6115–6134,  
505 <https://doi.org/10.5194/acp-22-6115-2022>, 2022.
- 506
- 507 Carn, S. A., Clarisse, L., & Prata, A. J. (2016). Multi-decadal satellite measurements of global volcanic degassing.  
508 *Journal of Volcanology and Geothermal Research*, 311, 99-134.
- 509
- 510 Carn, S. A., Newman, P. A., Aquila, V., Gonnermann, H., & Dufek, J. (2021). Anticipating climate impacts of major  
511 volcanic eruptions. *Eos*, 102.
- 512
- 513 Chahine, M., Barnet, C., Olsen, E. T., Chen, L., & Maddy, E. (2005). On the determination of atmospheric minor  
514 gases by the method of vanishing partial derivatives with application to CO<sub>2</sub>. *Geophysical Research*  
515 *Letters*, 32(22). <https://doi.org/https://doi.org/10.1029/2005GL024165>
- 516
- 517 Clarisse, L., Coheur, P.-F., Theys, N., Hurtmans, D., and Clerbaux, C.: The 2011 Nabro eruption, a SO<sub>2</sub> plume  
518 height analysis using IASI measurements, *Atmos. Chem. Phys.*, 14, 3095–3111,  
519 <https://doi.org/10.5194/acp-14-3095-2014>, 2014.
- 520
- 521 de Leeuw, J., Schmidt, A., Witham, C. S., Theys, N., Taylor, I. A., Grainger, R. G., Pope, R. J., Haywood, J.,  
522 Osborne, M., & Kristiansen, N. I. (2021). The 2019 Raikoke volcanic eruption -- Part 1: Dispersion model  
523 simulations and satellite retrievals of volcanic sulfur dioxide. *Atmospheric Chemistry and Physics*, 21(14),  
524 10851–10879. <https://doi.org/10.5194/acp-21-10851-2021>
- 525
- 526 Fairlie, T. D., Vernier, J.-P., Natarajan, M., & Bedka, K. M. (2014). Dispersion of the Nabro volcanic plume and its  
527 relation to the Asian summer monsoon. *Atmospheric Chemistry and Physics*, 14(13).





- 528 <https://doi.org/10.5194/acp-14-7045-2014>  
529  
530 Firstov, P. P., Popov, O. E., Lobacheva, M. A., Budilov, D. I., & Akbashev, R. R. (2020). *Wave perturbations in the*  
531 *atmosphere accompanied the eruption of the Raykoke volcano (Kuril Islands) 21--22 June, 2019.*  
532  
533  
534 Folch, A., Costa, A., and Macedonio, G.: FPLUME-1.0: An integral volcanic plume model accounting for ash  
535 aggregation, *Geosci. Model. Dev.*, 9, 431–450, <https://doi.org/10.5194/gmd9-431-2016>, 2016.
- 536 Fromm, M., Nedoluha, G., & Charvát, Z. (2013). Comment on “Large Volcanic Aerosol Load in the Stratosphere  
537 Linked to Asian Monsoon Transport.” *Science*, 339(6120), 647. <https://doi.org/10.1126/science.1228605>
- 538 Hedelt, P., Efremenko, D. S., Loyola, D. G., Spurr, R., and Clarisse, L.: Sulfur dioxide layer height retrieval from  
539 Sentinel-5 Precursor/TROPOMI using FP\_ILM, *Atmos. Meas. Tech.*, 12, 5503–5517,  
540 <https://doi.org/10.5194/amt-12-5503-2019>, 2019
- 541 Gorkavyi, N., Krotkov, N., Li, C., Lait, L., Colarco, P., Carn, S., DeLand, M., Newman, P., Schoeberl, M., Taha, G.,  
542 Torres, O., Vasilkov, A., & Joiner, J. (2021). Tracking aerosols and SO<sub>2</sub> clouds from the Raikoke eruption:  
543 3D view from satellite observations. *Atmospheric Measurement Techniques*, 14(12), 7545–7563.  
544 <https://doi.org/10.5194/amt-14-7545-2021>
- 545  
546 Gorshkov G S, 1970, *Volcanism and the Upper Mantle; Investigations in the Kurile Island Arc*, New York: Plenum  
547 Publishing Corp, 385 p.  
548
- 549 Harvey, N. J., Dacre, H. F., Saint, C., Prata, A. T., Webster, H. N., and Grainger, R. G.: Quantifying the impact of  
550 meteorological uncertainty on emission estimates and the risk to aviation using source inversion for the  
551 Raikoke 2019 eruption, *Atmos. Chem. Phys.*, 22, 8529–8545, <https://doi.org/10.5194/acp-22-8529-2022>,  
552 2022.  
553
- 554 Horváth, Á., Carr, J. L., Girina, O. A., Wu, D. L., Bril, A. A., Mazurov, A. A., Melnikov, D. V., Hoshyaripour, G.  
555 A., and Buehler, S. A.: Geometric estimation of volcanic eruption column height from GOES-R near-limb  
556 imagery – Part 1: Methodology, *Atmos. Chem. Phys.*, 21, 12189–12206, [https://doi.org/10.5194/acp-21-](https://doi.org/10.5194/acp-21-12189-2021)  
557 12189-2021, 2021a.
- 558  
559
- 560 Horváth, Á., Girina, O. A., Carr, J. L., Wu, D. L., Bril, A. A., Mazurov, A. A., Melnikov, D. V., Hoshyaripour, G.  
561 A., & Buehler, S. A. (2021). Geometric estimation of volcanic eruption column height from GOES-R near-  
562 limb imagery -- Part 2: Case studies. *Atmospheric Chemistry and Physics*, 21(16), 12207–12226.  
563 <https://doi.org/10.5194/acp-21-12207-2021b>



564

565

566

Hyman, D. M. and Pavolonis, M. J.: Probabilistic retrieval of volcanic SO<sub>2</sub> layer height and partial column density using the Cross-track Infrared Sounder (CrIS), *Atmospheric Measurement Techniques*, 13, 5891–5921, <https://doi.org/10.5194/amt-13-5891-2020>, 2020.

569

570

571

572

573

Inness, A., Ades, M., Balis, D., Efremenko, D., Flemming, J., Hedelt, P., Koukouli, M.-E., Loyola, D., and Ribas, R.: Evaluating the assimilation of S5P/TROPOMI near real-time SO<sub>2</sub> columns and layer height data into the CAMS integrated forecasting system (CY47R1), based on a case study of the 2019 Raikoke eruption, *Geosci. Model Dev.*, 15, 971–994, <https://doi.org/10.5194/gmd-15-971-2022>, 2022.

574

575

576

577

578

Jensen, E. J., Woods, S., Lawson, R. P., Bui, T. P., Pfister, L., Thornberry, T. D., Rollins, A. W., Vernier, J.-P., Pan, L. L., Honomichl, S., & Toon, O. B. (2018). Ash Particles Detected in the Tropical Lower Stratosphere. *Geophysical Research Letters*, 45(20). <https://doi.org/10.1029/2018GL079605>.

579

580

581

582

Khaykin, S.M., de Laat, A.T.J., Godin-Beekmann, S. *et al.* Unexpected self-lofting and dynamical confinement of volcanic plumes: the Raikoke 2019 case. *Sci Rep* 12, 22409 (2022). <https://doi.org/10.1038/s41598-022-27021-0>

583

584

585

586

587

Kloss, C., Berthet, G., Sellitto, P., Ploeger, F., Taha, G., Tidiga, M., Eremenko, M., Bossolasco, A., Jégou, F., Renard, J.-B., & Legras, B. (2021). Stratospheric aerosol layer perturbation caused by the 2019 Raikoke and Ulawun eruptions and their radiative forcing. *Atmospheric Chemistry and Physics*, 21(1), 535–560. <https://doi.org/10.5194/acp-21-535-2021>

588

589

590

591

Knepp, T. N., Thomason, L., Kovilakam, M., Tackett, J., Kar, J., Damadeo, R., and Flittner, D.: Identification of smoke and sulfuric acid aerosol in SAGE III/ISS extinction spectra, *Atmos. Meas. Tech.*, 15, 5235–5260, <https://doi.org/10.5194/amt-15-5235-2022>, 2022.

592

593

594

595

Kovilakam, M., Thomason, L. W., Ernest, N., Rieger, L., Bourassa, A., & Millán, L. (2020). The Global Space-based Stratospheric Aerosol Climatology (version 2.0): 1979–2018. *Earth System Science Data*, 12(4), 2607–2634. <https://doi.org/10.5194/essd-12-2607-2020>

596

597

598

LeGrande, A., Tsigaridis, K. & Bauer, S. Role of atmospheric chemistry in the climate impacts of stratospheric volcanic injections. *Nature Geosci* 9, 652–655 (2016). <https://doi.org/10.1038/ngeo2771>

599

600

Marshall, L., Johnson, J. S., Mann, G. W., Lee, L., Dhomse, S. S., Regayre, L., et al. (2019). Exploring how eruption source parameters affect volcanic radiative forcing using statistical emulation. *Journal of Geophysical*



- 601 Research: Atmospheres, 124, 964–985. <https://doi.org/10.1029/2018JD028675>
- 602
- 603 Marshall, L. R., Smith, C. J., Forster, P. M., Aubry, T. J., Andrews, T., & Schmidt, A. (2020). Large variations in  
604 volcanic aerosol forcing efficiency due to eruption source parameters and rapid adjustments. *Geophysical*  
605 *Research Letters*, 47, e2020GL090241. <https://doi.org/10.1029/2020GL090241>
- 606
- 607 Mastin, L. G.: A user-friendly one-dimensional model for wet volcanic plumes, *Geochem. Geophys. Geosy.*, 8,  
608 <https://doi.org/10.1029/2006GC001455>, 2007.
- 609
- 610 McKeen, S.A., Liu, S.C. and Kiang, C.S., 1984. On the chemistry of stratospheric SO<sub>2</sub> from volcanic eruptions.  
611 *Journal of Geophysical Research: Atmospheres*, 89(D3), pp.4873-4881.  
612
- 613
- 614 Mills, M. J., et al. (2016), Global volcanic aerosol properties derived from emissions, 1990–2014, using  
CESM1(WACCM), *J. Geophys. Res. Atmos.*, 121, 2332–2348, doi:10.1002/2015JD024290.
- 615
- 616 Millán, L., Santee, M. L., Lambert, A., Livesey, N. J., Werner, F., Schwartz, M. J., et al. (2022). The Hunga Tonga-  
617 Hunga Ha'apai Hydration of the Stratosphere. *Geophysical Research Letters*, 49,  
e2022GL099381. <https://doi.org/10.1029/2022GL099381>
- 618
- 619 Mingari, L., Folch, A., Prata, A. T., Pardini, F., Macedonio, G., and Costa, A.: Data assimilation of volcanic aerosol  
620 observations using FALL3D+PDAF, *Atmos. Chem. Phys.*, 22, 1773–1792, [https://doi.org/10.5194/acp-22-](https://doi.org/10.5194/acp-22-1773-2022)  
621 1773-2022, 2022.
- 622
- 623 Müller, W. A., Jungclaus, J. H., Mauritsen, T., Baehr, J., Bittner, M., Budich, R., et al. (2018). A higher-resolution  
624 version of the Max Planck Institute Earth System Model (MPI-ESM1.2-HR). *Journal of Advances in*  
*Modeling Earth Systems*, 10, 1383–1413. <https://doi.org/10.1029/2017MS001217>
- 625
- 626
- 627 Muser, L. O., Hoshyaripour, G. A., Bruckert, J., Horváth, Á., Malinina, E., Wallis, S., Prata, F. J., Rozanov, A., von  
628 Savigny, C., Vogel, H., & Vogel, B. (2020). Particle aging and aerosol-radiation interaction affect volcanic  
629 plume dispersion: evidence from the Raikoke 2019 eruption. *Atmospheric Chemistry and Physics*, 20(23),  
630 15015–15036. <https://doi.org/10.5194/acp-20-15015-2020>
- 631
- 632
- 633 Osborne, M. J., de Leeuw, J., Witham, C., Schmidt, A., Beckett, F., Kristiansen, N., Buxmann, J., Saint, C., Welton,  
634 E. J., Fochesatto, J., Gomes, A. R., Bundke, U., Petzold, A., Marengo, F., & Haywood, J. (2022). The 2019  
635 Raikoke volcanic eruption - Part 2: Particle-phase dispersion and concurrent wildfire smoke emissions.



- 636 *Atmospheric Chemistry and Physics*, 22(5), 2975–2997. <https://doi.org/10.5194/acp-22-2975-2022>
- 637
- 638 Petracca, I., De Santis, D., Picchiani, M., Corradini, S., Guerrieri, L., Prata, F., Merucci, L., Stelitano, D., Del Frate,  
639 F., Salvucci, G., and Schiavon, G.: Volcanic cloud detection using Sentinel-3 satellite data by means of  
640 neural networks: the Raikoke 2019 eruption test case, *Atmos. Meas. Tech.*, 15, 7195–7210,  
641 <https://doi.org/10.5194/amt-15-7195-2022>, 2022.
- 642
- 643 Prata, A. J., & Bernardo, C. (2007). Retrieval of volcanic SO<sub>2</sub> column abundance from Atmospheric Infrared  
644 Sounder data. *Journal of Geophysical Research: Atmospheres*, 112(D20).  
645 <https://doi.org/https://doi.org/10.1029/2006JD007955>
- 646
- 647 Prata, A. T., Mingari, L., Folch, A., Macedonio, G., and Costa, A.: FALL3D-8.0: a computational model for  
648 atmospheric transport and deposition of particles, aerosols and radionuclides – Part 2: Model validation,  
649 *Geosci. Model Dev.*, 14, 409–436, <https://doi.org/10.5194/gmd-14-409-2021>, 2021.
- 650
- 651 Prata, A. T., Grainger, R. G., Taylor, I. A., Povey, A. C., Proud, S. R., and Poulsen, C. A.: Uncertainty-bounded  
652 estimates of ash cloud properties using the ORAC algorithm: application to the 2019 Raikoke eruption,  
653 *Atmos. Meas. Tech.*, 15, 5985–6010, <https://doi.org/10.5194/amt-15-5985-2022>, 2022.
- 654
- 655 Sawamura, P., Vernier, J. P., Barnes, J. E., Berkoff, T. A., Welton, E. J., Alados-Arboledas, L., Navas-Guzmán, F.,  
656 Pappalardo, G., Mona, L., Madonna, F., Lange, D., Sicard, M., Godin-Beekmann, S., Payen, G., Wang, Z.,  
657 Hu, S., Tripathi, S. N., Cordoba-Jabonero, C., & Hoff, R. M. (2012). Stratospheric AOD after the 2011  
658 eruption of Nabro volcano measured by lidars over the Northern Hemisphere. *Environmental Research*  
659 *Letters*, 7(3). <https://doi.org/10.1088/1748-9326/7/3/034013>
- 660
- 661 Sellitto, P., Podglajen, A., Belhadji, R., Boichu, M., Carboni, E., Cuesta, J., Duchamp, C., Kloss, C., Siddans, R.,  
662 Bègue, N., Blarel, L., Jegou, F., Khaykin, S., Renard, J.-B., & Legras, B. (2022). The unexpected radiative  
663 impact of the Hunga Tonga eruption of 15th January 2022. *Communications Earth & Environment*, 3(1), 288.  
664 <https://doi.org/10.1038/s43247-022-00618-z>
- 665
- 666 Sennert, 2019. Global Volcanism Program, 2019. Report on Raikoke (Russia). Weekly Volcanic Activity Report, 26  
June-2 July 2019. Smithsonian Institution and US Geological Survey.
- 667
- 668 Schmidt, A., et al. (2018). Volcanic radiative forcing from 1979 to 2015. *Journal of Geophysical Research:*  
669 *Atmospheres*, 123(22), 12491-12508.
- 670
- 671 Schmidt, A., Aubry, T.J., Rigby, R., Stevenson, J. and Loughlin, S., Volc2Clim online tool, 2023,  
672 <https://doi.org/10.5281/zenodo.7602062>, <https://volc2clim.bgs.ac.uk/>.



- 673  
674 Smith, C. J., Forster, P. M., Allen, M., Leach, N., Millar, R. J., Passerello, G. A., & Regayre, L. A. (2018). FAIR  
675 v1.3: a simple emissions-based impulse response and carbon cycle model. *Geoscientific Model*  
676 *Development*, 11(6), 2273–2297. <https://doi.org/10.5194/gmd-11-2273-2018>  
677  
678 Stenchikov, G., Ukhov, A., Osipov, S., Ahmadov, R., Grell, G., Cady-Pereira, K., et al. (2021). How does a  
679 Pinatubo-size volcanic cloud reach the middle stratosphere? *Journal of Geophysical Research:*  
680 *Atmospheres*, 126, e2020JD033829. <https://doi.org/10.1029/2020JD033829>  
681  
682 Theys, N., Campion, R., Clarisse, L., Brenot, H., van Gent, J., Dils, B., Corradini, S., Merucci, L., Coheur, P.-F.,  
683 Van Roozendael, M., Hurtmans, D., Clerbaux, C., Tait, S., & Ferrucci, F. (2013). Volcanic SO<sub>2</sub> fluxes  
684 derived from satellite data: a survey using OMI, GOME-2, IASI and MODIS. *Atmospheric Chemistry and*  
685 *Physics*, 13(12), 5945–5968. <https://doi.org/10.5194/acp-13-5945-2013>  
686  
687 Theys, N., De Smedt, I., Yu, H., Danckaert, T., van Gent, J., Hörmann, C., Wagner, T., Hedelt, P., Bauer, H.,  
688 Romahn, F., Pedernana, M., Loyola, D., & Van Roozendael, M. (2017). Sulfur dioxide retrievals from  
689 TROPOMI onboard Sentinel-5 Precursor: algorithm theoretical basis. *Atmospheric Measurement*  
690 *Techniques*, 10(1), 119–153. <https://doi.org/10.5194/amt-10-119-2017>  
691  
692 Theys, N., Fioletov, V., Li, C., De Smedt, I., Lerot, C., McLinden, C., Krotkov, N., Griffin, D., Clarisse, L., Hedelt,  
693 P., Loyola, D., Wagner, T., Kumar, V., Innes, A., Ribas, R., Hendrick, F., Vlietinck, J., Brenot, H., & Van  
694 Roozendael, M. (2021). A sulfur dioxide Covariance-Based Retrieval Algorithm (COBRA): application to  
695 TROPOMI reveals new emission sources. *Atmospheric Chemistry and Physics*, 21(22), 16727–16744.  
696 <https://doi.org/10.5194/acp-21-16727-2021>  
697  
698 Theys, N., Lerot, C., Brenot, H., van Gent, J., De Smedt, I., Clarisse, L., Burton, M., Varnam, M., Hayer, C., Esse,  
699 B., & Van Roozendael, M. (2022). Improved retrieval of SO<sub>2</sub> plume height from TROPOMI using an  
700 iterative Covariance-Based Retrieval Algorithm. *Atmospheric Measurement Techniques*, 15(16), 4801–  
701 4817. <https://doi.org/10.5194/amt-15-4801-2022>  
702  
703  
704 Tournigand, P.-Y., Cigala, V., Lasota, E., Hammouti, M., Clarisse, L., Brenot, H., Prata, F., Kirchengast, G.,  
705 Steiner, A. K., & Biondi, R. (2020). A multi-sensor satellite-based archive of the largest SO<sub>2</sub> volcanic  
706 eruptions since 2006. *Earth System Science Data*, 12(4), 3139–3159. [https://doi.org/10.5194/essd-12-3139-](https://doi.org/10.5194/essd-12-3139-2020)  
707 2020  
708  
709 Vaughan, G., Wareing, D., and Ricketts, H.: Measurement Report: Lidar measurements of stratospheric aerosol



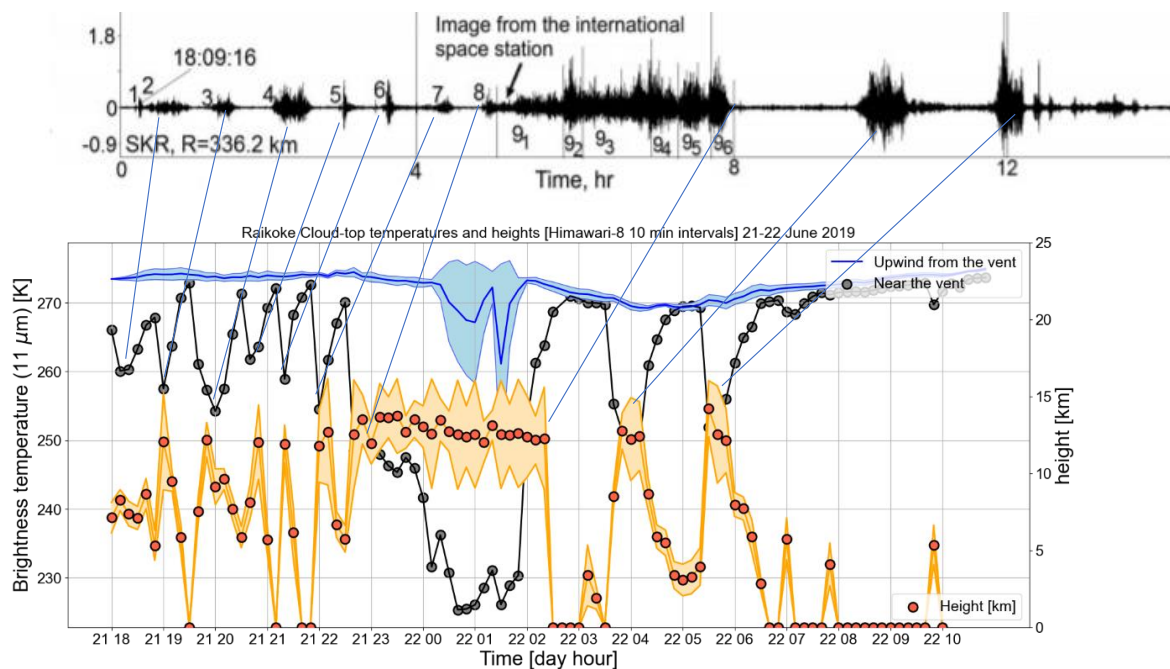
- 710 following the 2019 Raikoke and Ulawun volcanic eruptions, *Atmos. Chem. Phys.*, 21, 5597–5604,  
711 <https://doi.org/10.5194/acp-21-5597-2021>, 2021.
- 712
- 713 Veefkind, J. P., Aben, I., McMullan, K., Förster, H., de Vries, J., Otter, G., Claas, J., Eskes, H. J., de Haan, J. F.,  
714 Kleipool, Q., van Weele, M., Hasekamp, O., Hoogeveen, R., Landgraf, J., Snel, R., Tol, P., Ingmann, P.,  
715 Voors, R., Kruizinga, B., ... Levelt, P. F. (2012). TROPOMI on the ESA Sentinel-5 Precursor: A GMES  
716 mission for global observations of the atmospheric composition for climate, air quality and ozone layer  
717 applications. *Remote Sensing of Environment*, 120, 70–83.  
718 <https://doi.org/https://doi.org/10.1016/j.rse.2011.09.027>
- 719
- 720 Vernier, J.-P., Fairlie, T. D., Deshler, T., Natarajan, M., Knepp, T., Foster, K., Wienhold, F. G., Bedka, K. M.,  
721 Thomason, L., & Trepte, C. (2016). In situ and space-based observations of the Kelud volcanic plume: The  
722 persistence of ash in the lower stratosphere. *Journal of Geophysical Research*, 121(18).  
723 <https://doi.org/10.1002/2016JD025344>
- 724
- 725 Vernier, J.-P., Fairlie, T. D., Murray, J. J., Tupper, A., Trepte, C., Winker, D., Pelon, J., Garnier, A., Jumelet, J.,  
726 Pavolonis, M., Omar, A. H., & Powell, K. A. (2013). An advanced system to monitor the 3D structure of  
727 diffuse volcanic ash clouds. *Journal of Applied Meteorology and Climatology*, 52(9).  
728 <https://doi.org/10.1175/JAMC-D-12-0279.1>
- 729
- 730 Vömel H, Evan S, Tully M. Water vapor injection into the stratosphere by Hunga Tonga-Hunga Ha'apai. *Science*.  
731 2022 Sep 23;377(6613):1444-1447. doi: 10.1126/science.abq2299. Epub 2022 Sep 22. PMID: 36137033.
- 732
- 733 Winker, D. M., Tackett, J. L., Getzewich, B. J., Liu, Z., Vaughan, M. A., & Rogers, R. R. (2013). The global 3-D  
734 distribution of tropospheric aerosols as characterized by CALIOP. *Atmospheric Chemistry and Physics*, 13(6),  
735 3345–3361. <https://doi.org/10.5194/acp-13-3345-2013>
- 736 Winker, D. M., Pelon, J., Coakley, J. A., Ackerman, S. A., Charlson, R. J., Colarco, P. R., Flamant, P., Fu, Q., Hoff,  
737 R. M., Kittaka, C., Kubar, T. L., Le Treut, H., McCormick, M. P., Mégie, G., Poole, L., Powell, K., Trepte,  
738 C., Vaughan, M. A., & Wielicki, B. A. (2010). The CALIPSO Mission. *Bulletin of the American*  
739 *Meteorological Society*, 91(9), 1211–1230. <https://doi.org/10.1175/2010BAMS3009.1>
- 740
- 741 Zängl, G., Reinert, D., Rípodas, P., and Baldauf, M.: The ICON (ICOsahedral Non-hydrostatic) modelling  
742 framework of DWD and MPI-M: Description of the non-hydrostatic dynamical core, *Q. J. Roy. Meteor.*  
743 *Soc.*, 141, 563–579, <https://doi.org/10.1002/qj.2378>, 2015. a, b, c
- 744
- 745 Zhu, Y., Toon, O.B., Jensen, E.J. et al. Persisting volcanic ash particles impact stratospheric SO<sub>2</sub> lifetime and  
746 aerosol optical properties. *Nat Commun* 11, 4526 (2020). <https://doi.org/10.1038/s41467-020-18352-5>



750 **Figures.**

751

752



753

754 **Figure 1. (Top) Modified from Fig.7 from (Firstov et al., 2020) showing IS signals during the first 12h after**  
755 **the beginning of the Raikoke eruption which started near 18 UTC on June 21 2019. (Bottom) A time series of**  
756 **corresponding Brightness Cloud Top Temperature at 11µm derived from HIMWARI-8 is shown. Height**  
757 **retrievals near the vent (orange data points) and uncertainties (orange shaded region) taken from Prata et al.**  
758 **(2022).**

759

760

761

762

763

764

765

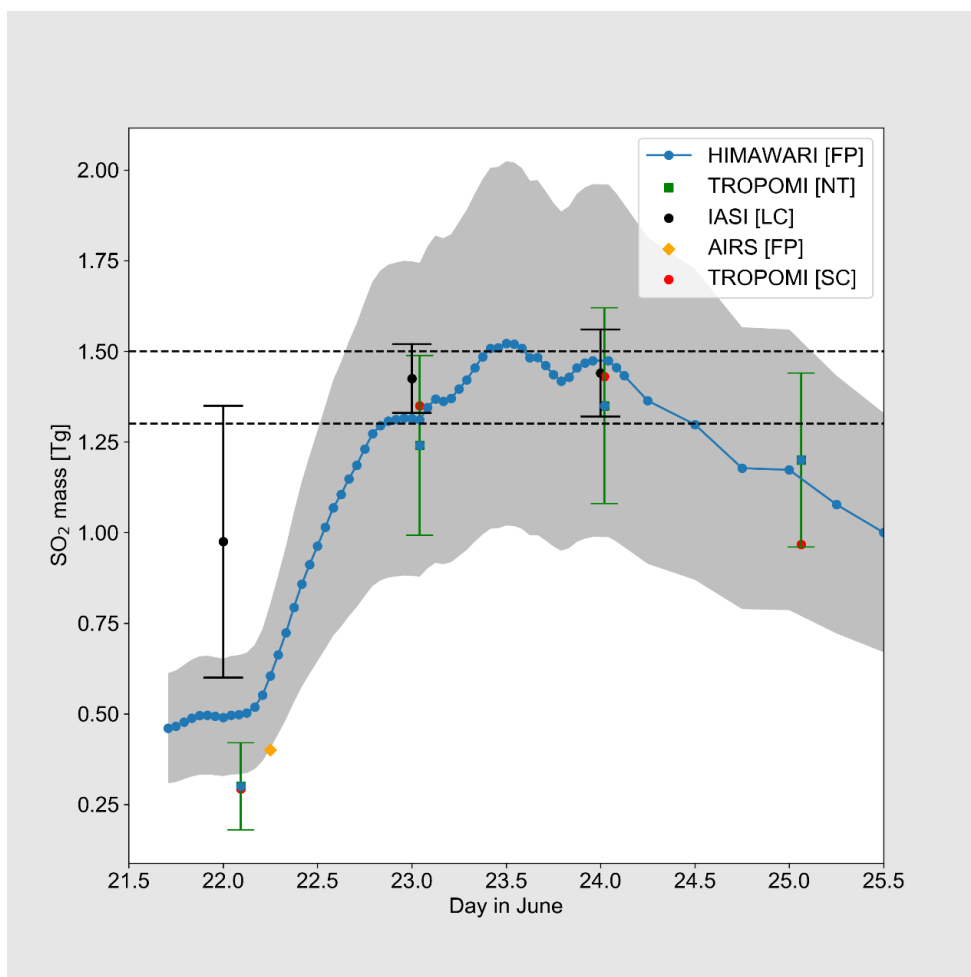
766

767





768



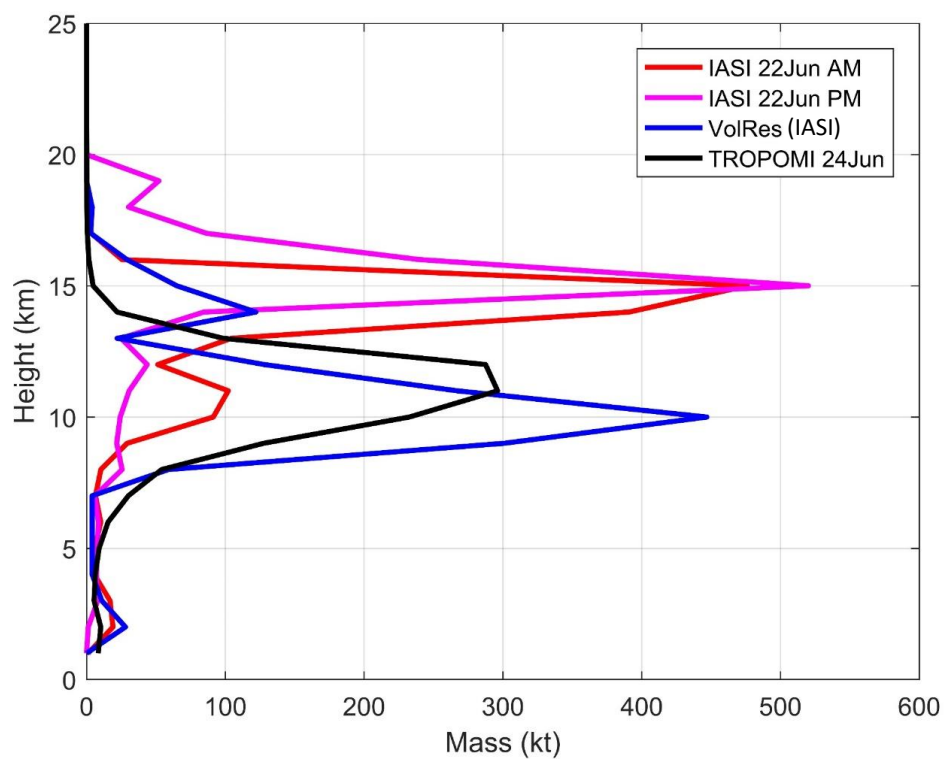
769

770 **Figure 2. Total SO<sub>2</sub> mass (Tg) as a function of time in June 2019 estimated from various satellite sensors for**  
771 **the eruption of Raikoke. The grey-colored region indicates the uncertainty range of the Himawari-8 (AHI)**  
772 **retrievals. A ±20% uncertainty has been placed on the TROPOMI estimates. The IASI estimates come from**  
773 **different satellites and times of day (day/night); the vertical lines on these data indicate the range of the**  
774 **estimations. Himawari-8 samples every 10 minutes. After 24 June retrievals were performed at longer**  
775 **intervals. Distributed to VolRes on 06/28/2019.**

776

777

778



779

780 **Figure 3: SO<sub>2</sub> mass altitude distribution from IASI (refined analysis), VolRes (IASI initial estimate) and**  
781 **TROPOMI. The associated data is provided in Table 1.**

782

783

784

785

786

787

788

789

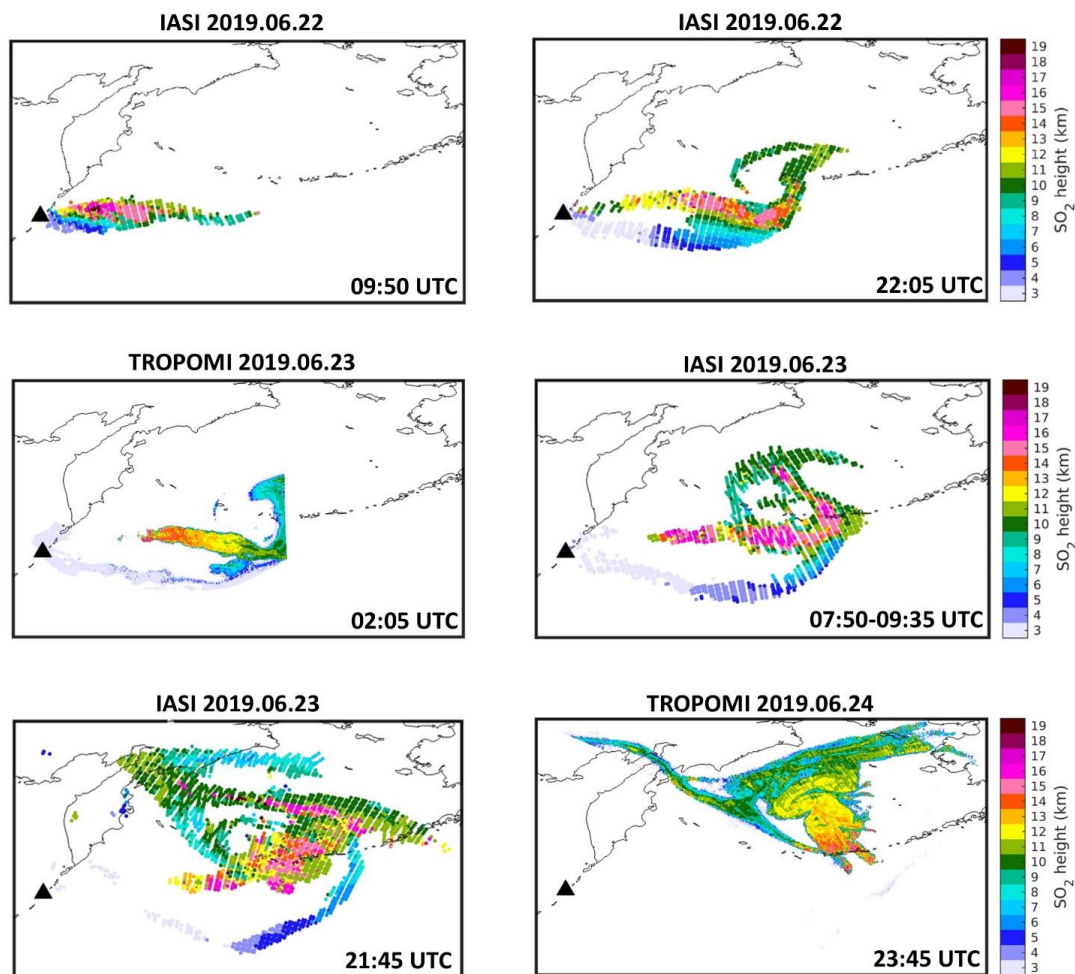
790

791

792



793



794

795 **Figure 4: Examples of SO<sub>2</sub> height retrievals from IASI (refined analysis) and TROPOMI for Raikoke eruption**  
796 **for 22-24 June 2019. The Raikoke volcano is marked by a black triangle. Approximate overpass times are**  
797 **indicated in each panel.**

798

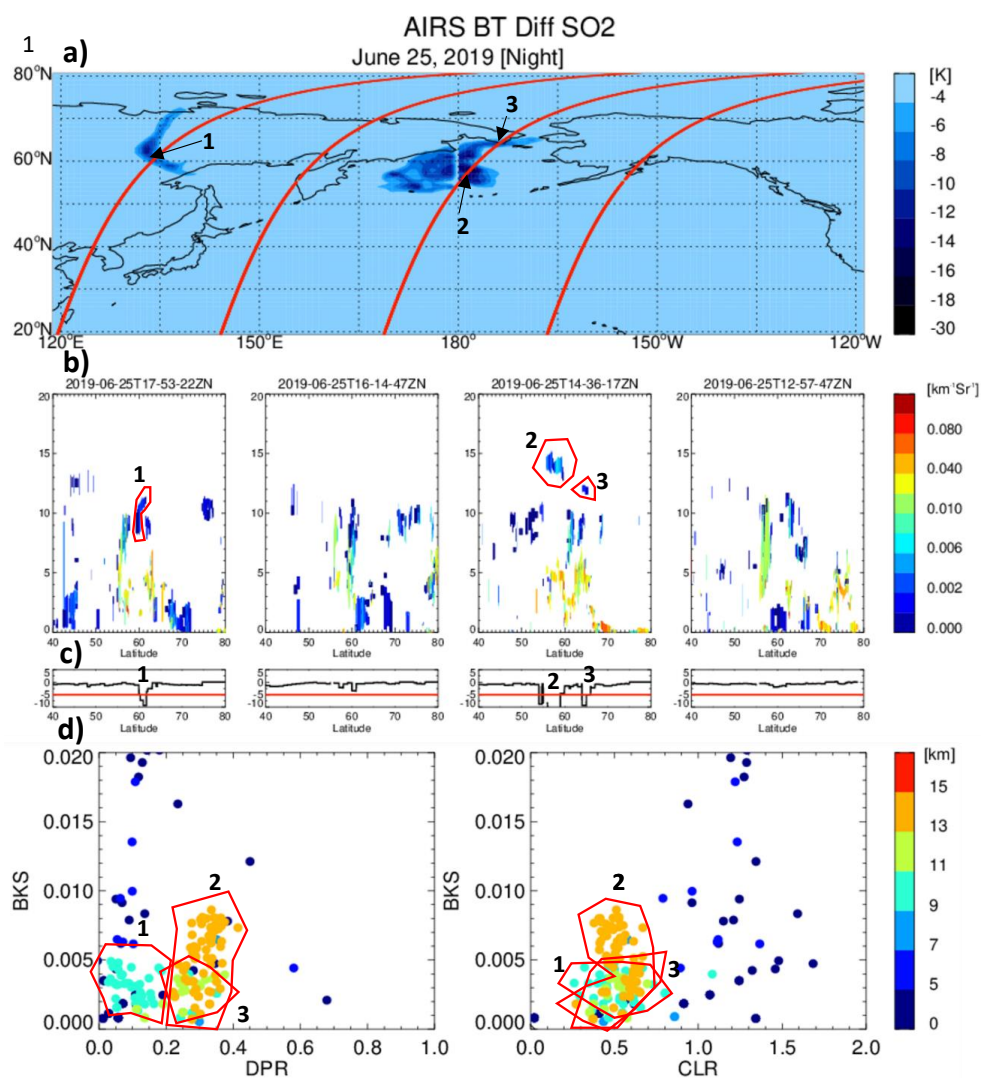
799

800

801

802

803



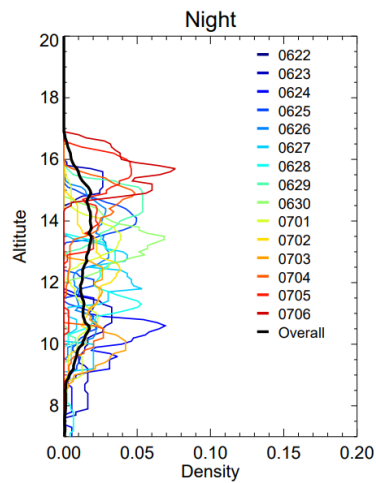
804

805 **Figure 5. (a) AIRS Nighttime Brightness Temperature Difference (BTD) ( $1361.44\text{-}1433.06\text{ cm}^{-1}$ ) on 25 June**  
 806 **2022 together with 4 CALIOP ground-tracks (red). (b) Corresponding aerosol and cloud layer products from**  
 807 **CALIOP level 2V4.2 product and (c) extracted AIRS BTD extracted along the CALIOP orbit tracks. (d)**  
 808 **diagrams of particulate backscatter (BKS) as a function of mean layer particulate DePolarization Ratio (DPR)**  
 809 **(left) and particulate CoLor Ratio (CLR) (right) derived from CALIOP and colored by mid-layer altitudes.**

810

811

812



813

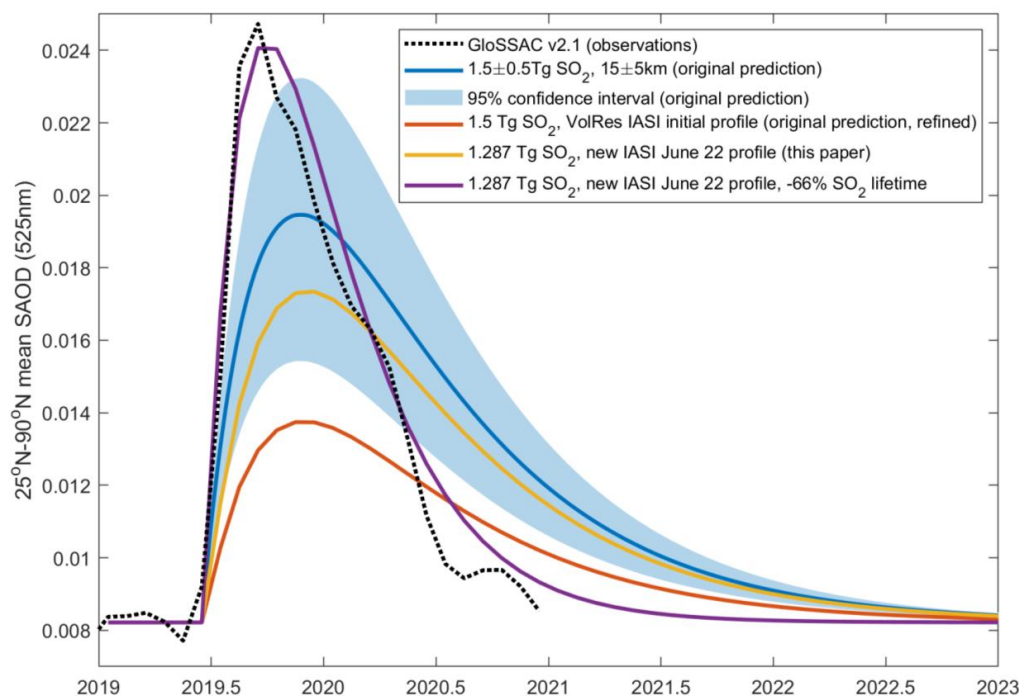
814 **Figure 6. Daily nighttime Probability Density Function profiles of the mid-layer geometric altitude for volcanic**  
815 **layers observed by CALIOP/AIRS using plume identification criterion when DPR < 0.4 and CLR < 0.7 and**  
816 **altitude > 5km and BTD < -6K between 06/22 and 07/06. The black line is the overall pdf profile using all**  
817 **nighttime data between 06/22 and 07/06.**

818

819

820

821



822

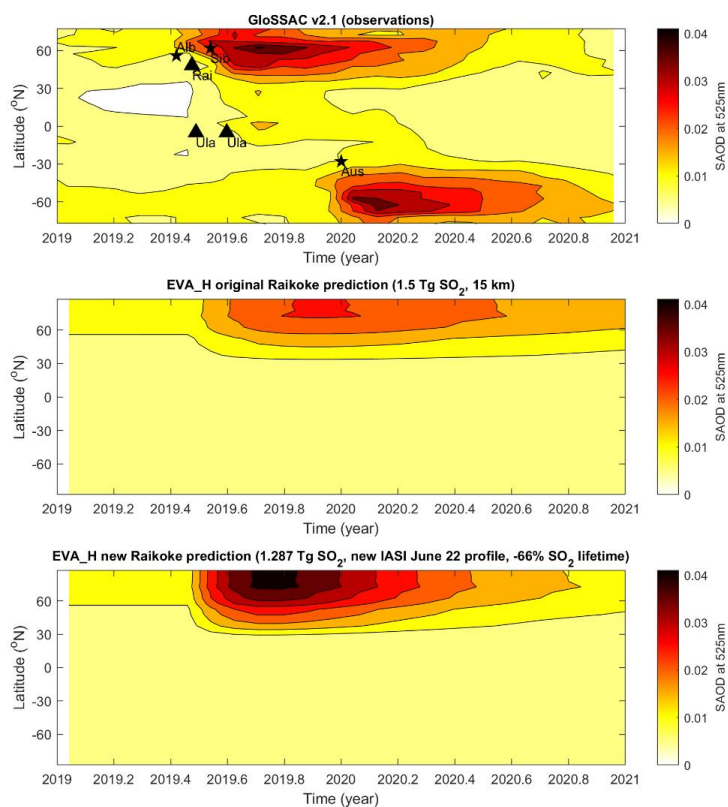
823 **Figure 7: Northern Hemisphere (25°N-90°N) monthly-mean SAOD at 525nm as projected by EVA\_H**  
 824 **(continuous colored lines) and observed (GloSSAC v2.1, black dashed line). The light blue shading and line**  
 825 **shows the first projection made at the time of the eruption and its confidence interval based on an injection**  
 826 **height of 15+/-5km and SO<sub>2</sub> mass of 1.5+/-0.5 Tg. The yellow line shows the second projection made at the**  
 827 **time of the eruption using the VolRes IASI initial profile. The orange line shows a new projection using the**  
 828 **new VolRes IASI June 22 profile presented in this study (Figure 3). The violet line uses the same profile, but**  
 829 **the SO<sub>2</sub>-to-aerosol conversion timescale in EVA\_H reduced by 66%.**

830

831

832

833



834

835 **Figure 8: SAOD at 525nm as observed (GloSSAC v2.1, top) and projected by EVA\_H following the Raikoke**  
836 **2019 eruption (middle) and using the revised IASI June 22 SO<sub>2</sub> profile presented in this paper along with the**  
837 **adjusted (-66%) SO<sub>2</sub>-to-aerosol conversion timescale in EVA\_H (bottom). EVA\_H was run only with the**  
838 **Raikoke injections, and not with injections associated with the Ulawun 2019 eruptions (denoted by black**  
839 **triangles in the top panel) nor with wildfire events in Alberta, Siberia (2019) and Australia (2020) (denoted by**  
840 **black stars in the top panel).**

841

842

843

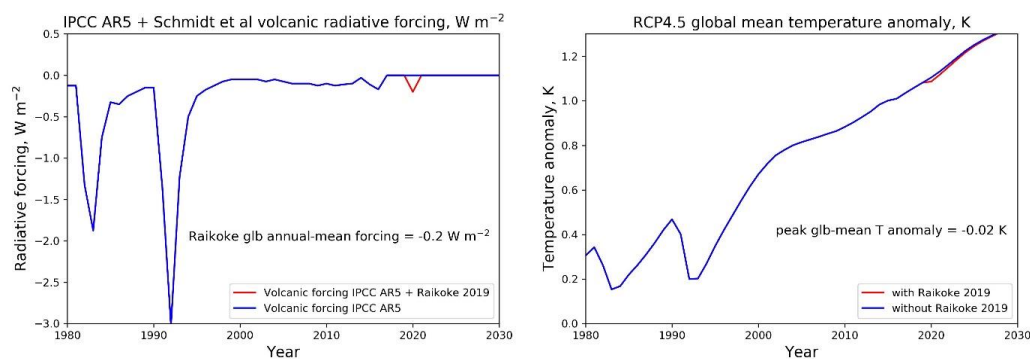
844

845

846

847





848

849 **Figure 9: Annual global mean volcanic radiative forcing (left) and corresponding annual global mean surface**  
850 **temperature anomaly calculated using the climate response model FaIR (Smith et al., 2018) (right). Blue and**  
851 **red lines show results with and without accounting for the 2019 Raikoke eruption, respectively. This is the**  
852 **original figure shared on the VolRes mailing list on 06/26/19.**

853

854

855

856

857

858

859

860

861

862

863

864

865

866

867

868

869

870

871



872

Altitude	VolRes IASI initial profile	IASI 22 June 2019 (AM)	IASI 22 June 2019 (PM)	TROPOMI 24 June 2019
1	0	1.1	0	8.4
2	28	19.0	1.2	10.2
3	11	16.9	8	5.4
4	4	5.6	7.1	6.3
5	4	6.0	7.9	9.0
6	4	10.2	8.5	15.5
7	4	6.4	6.0	30.1
8	59	10.3	25.6	54.1
9	301	29.2	21.7	127.6
10	446	91.3	24.2	232.6
11	266	102.1	30.7	296.2
12	128	51.3	43.7	287.5
13	22	104.4	24.8	98.4
14	122	390.9	84.5	22.0
15	65	476.2	520.2	4.7
16	29	25.5	239.7	1.63
17	3	3.3	86.4	0.53
18	4	2.6	30.2	0.19
19	0	0	52.1	0.14
20	0	0	0	0.1
<b>Total</b>	<b>1500 kt (scaled)</b>	<b>1352.3 kt</b>	<b>1222.5 kt</b>	<b>1210.6 kt</b>

873

874 **Table 1: SO<sub>2</sub> mass profile (in kt) derived from IASI and TROPOMI for the Raikoke eruption.**

875



Date	Data type	Activities	Data variables	Platform	Add. Information
06/24	Satellite	SO2 and plume height maps 06/24 & 06/25	SO2 total column (DU) and concentration (ppmv ?)	TROPOMI /Sentinel 5P	Polar Orbit/ESA
06/24	Satellite	Aerosol maps and profiles when ?	Aerosol extinction (km-1)	NPP/OMPS	Polar Orbit/NASA
06/25	Satellite	SO2 maps 06/21 & 06/22	SO2 total column (DU)	Metop/IASI	Polar Orbit/Eumetsat
06/25	Satellite	Ash and SO2 total column	Ash signature (11-12 um) and SO2 UTLS (VCD DU)	AHI/HIMAWARI-8	Geo Orbit/JAXA
06/25	Satellite	Plume heights and optical properties	Backscatter and depolarization at 532 and 1064 nm	CALIOP/CALIPSO	Polar Orbit/NASA
06/25	Satellite	Maps of plume height and properties 06/23	Height (km) and AOD, angstrom coeff, SSA	MISR/Terra	Polar Orbit/NASA
06/25	Model	Volcanic plume maps at 100 and 140 hPa	Aerosol extinction at XX nm	WACCM	Model type
06/25	Model	Impacts on stratospheric aerosol	Stratospheric AOD	GEOS-5	
06/26	Satellite	Mass distribution profile on 06/23	Mass per levels (kt)	TROPOMI/Sentinel 5P	Polar Orbit/ESA
06/26	Satellite	SO2 plume vertical information	SO2 mixing ratio (ppbv)	MLS/Aura	Polar Orbit/ESA
06/26	Model	Radiative and climate impacts	RF TOA (w/m2)	??	
06/28	Model	Trajectory simulation of Raikoke dispersion	Plume height (km)	Langley Trajectory Model	GEOS-5 wind data
07/03	Satellite	Plume height and properties	Backscatter and depolarization at 532 and 1064 nm	CALIOP/CALIPSO	Polar Orbit/ESA
07/09	Model	SO2 and ash plume dispersion 06/21 to 06/25	Ash and SO2 mass concentration	ICONN-ART	
07/10	Ground-based lidar	Vertical plume profiles 07/05	Scattering ratio at 532 nm	OHP/LTA	
07/10	Satellite	Plume height and properties	Backscatter and depolarization at 532 and 1064 nm	CALIOP/CALIPSO	Polar Orbit/NASA
07/10	Satellite	Latitudinal time series	Aerosol extinction (km-1)	NPP/OMPS	NASA
07/16	Satellite	Animation of aerosol maps at 12.5 km, 13.5 km, 14.5 km and 16.5 km across the NH. 06/11 to 07/14	Aerosol extinction (km-1)	OMPS/NPP	Polar Orbit/NASA
07/17	Ground-based lidar	Volcanic aerosol profiles 06/29 and 07/08	RSC 1064 nm	SIRTA	
07/19	Satellite	Maps of SO2 centered in Indonesia/Australia (from 06/26 to 07/12), Ulawun eruption	SO2 DU	TROPOMI /Sentinel 5P	Polar Orbit/ESA
07/20	Satellite	Animation of aerosol maps at 18.5 km from 06/27 to 07/17	Aerosol extinction (km-1) at 674 nm	OMPS/NPP	Polar Orbit/NASA
07/21	Ground-based lidar	Volcanic aerosol profiles on 07/18 and 07/20	Scattering Ratio at 532 nm	OHP LTA	
08/07	Satellite	Animation of aerosol maps at 20.5 km	Aerosol extinction (km-1) at 674 nm	OMPS/NPP	Polar Orbit/NASA
08/24	Satellite	Volcanic plumes cross-section 11-20 Aug 2019	Scattering Ratio at 532 nm	CALIOP/CALIPSO	Polar Orbit/NASA
09/04	Balloon	Aerosol concentration profiles on 08/26 in Wyoming	Aerosol concentration for r>0.005 um, 0.092, 0.15, 0.28	Balloon	WOPC
09/17	Ground-	Atmospheric profiles of aerosols and	Backscatter profiles at 532 nm	Lidar LOA	

876

877

878 **Table 2: VolRes activities during the first 2 months after the Raikoke eruption.**